UNIVERSITY OF MARYLAND CONTRIBUTIONS

TO THE

13th INTERNATIONAL COSMIC RAY CONFERENCE

August 17-30, 1973, Denver, Colo.

Technical Report Nos. 73-131 thru 138

UNIVERSITY OF MARYLAND
DEPARTMENT OF PHYSICS AND ASTRONOMY
COLLEGE PARK, MARYLAND

Space Physics Group

UNIVERSITY OF MARYLAND CONTRIBUTIONS

TO THE

13th INTERNATIONAL COSMIC RAY CONFERENCE

August 17-30, 1973, Denver, Colo.

Technical Report Nos. 73-131 thru 138

Space Physics Group

TABLE OF CONTENTS

Technical Report #73-131

COSMIC RAY HYSTERESIS AS EVIDENCE FOR TIME-DEPENDENT DIFFUSIVE PROCESSES IN THE LONG TERM SOLAR MODULATION

J.J. O'Gallagher

Department of Physics and Astronomy, University of Maryland

College Park, Maryland (USA) 20742

A simple one-dimensional time-dependent diffusion-convection model for the modulation of cosmic rays is presented. This model predicts that the observed intensity $U(t_o)$ at a given time t_o is approximately equal to the intensity given by the time independent diffusion convection solution under interplanetary conditions which existed a time τ in the past, $[U(t_o) = U_S(t_o-\tau)]$, where τ is the average time spent by a particle inside the modulating cavity. Delay times in excess of several hundred days are possible with reasonable modulation parameters. Interpretation of phase lags observed during the 1969-70 solar maximum in terms of this model suggests that the modulating region is probably not less than 10 a.u. and maybe as much as 35 a.u. in extent.

1. Introduction. Observations of the time behavior of modulated cosmic rays have revealed that the integral intensities above different energy thresholds are not modulated in phase, particularly near times of solar maximum or minimum (Simpson 1963; Simpson and Wang, 1970; Balasubramanyan et al., 1968; Kane and Winkler, 1969). That is, regression plots between the modulated intensities at different energies sometimes exhibit a double-valued "loop" which recently has come to be called the "hysteresis effect" in cosmic rays. A number of recent studies of this behavior during the past solar maximum in 1969-1970 have shown that the effect exists for electrons as well as nuclei (Schmidt, 1972; Burger and Schwannenberg, 1973), and that protons and helium nuclei are affected differently in a way which depends on particle rigidity (Van Hollebeke, Wang and McDonald, 1972 and Rygg, O'Gallagher and Earl, 1973).

Some success in explaining this behavior in terms of the diffusion convection modulation model (Parker, 1963, 1965) has been achieved by invoking a diffusion coefficient κ whose dependence on particle magnetic rigidity R varies with time (Schmidt, 1972) or with heliocentric radius (Burger and Schwannenberg, 1973) or both (Van Hollebeke, et al., 1972). However as has been pointed out by Rygg, et al., 1973 all such models are fundamentally equivalent providing no observational characteristics which can distinguish between them. Furthermore, all involve the introduction of several new free parameters in order to provide sufficient flexibility to fit the wide range of observed behavior. It is fundamental to each of these approaches that the observed spectrum at a particular time is the solution to a Fokker-Planck equation under equilibrium conditions i.e. a stationary solution in which all time dependent effects are neglected.

However since the periods of solar maximum and solar minimum are probably not equilibrium situations it is instructive to consider an

analysis based on an alternate model in which the effects of time dependent diffusion are included as a first order correction. The model is very simple, being based on one dimensional time dependent diffusion which neglects all energy loss effects. However the basic conceptions are easily visualized and lead to the interpretation of "hysteresis" as a real rigidity dependent time lag in the modulated intensity at different rigidities. The model involves no new parameters and provides a basis for using hysteresis to measure some of the dynamical characteristics of the modulating region. In particular, when applied in a simple minded fashion to the balloon observations of hysteresis reported by Rygg et al., (1973) it provides a crude estimate of the distance in the boundary of the modulating region of between 10 and 20 astronomical units (a.u.). However when the limiting behavior at small diffusion coefficients is taken into account the model suggests that these observations are more consistent with a modulating region as large as 35 a.u. with a larger diffusion coefficient than is usually assumed.

2. Simple Model Including Time Dependent Diffusion. The basic features of the model are as follows

(1) The modulation is treated in a one dimensional solar wind so that the basic coordinate is the distance X inside the boundary.

(2) There are no energy loss effects (a consequence of one dimensional propagation) so that the behavior of the modulated differential density U(T) at a particular kinetic energy T can be analyzed independently of the behavior at other energies.

(3) The modulation at a particular energy depends on three very sbwly varying parameters [i] the distance X from the boundary; [ii] the diffusion coefficient κ which is taken to be independent of position inside the boundary for simplicity; [iii] the solar wind velocity V which is independent of position.

Subject to these conditions the modulated density U(X,t) at time t obeys a time dependent Fokker-Planck equation of the form

$$\frac{\partial U}{\partial t} = \kappa \frac{\partial^2 U}{\partial X^2} - V \frac{\partial U}{\partial X} \qquad (1)$$

Parker (1965) has analyzed the solution to equation (1) in terms of the probability density for finding a particle which crosses the boundary (X = 0) at t = 0 inside the boundary at X > 0 and t > 0. With a small change in notation we can write Parkers solution for a single particle in the diffusion approximation as:

$$P(X,V,\kappa,t) = \frac{X}{(4\pi\kappa t)^{\frac{1}{2}} t} \left\{ e^{\frac{-(Vt + X)^2}{4\kappa t}} \right\} \qquad (2)$$

where P is the probability density for finding a particle at X and t given that it is at the boundary at t = 0. Assuming a constant particle density U_o at the boundary, the density observed at X and t_o is then

$$U(X,t_o) = \int_{-\infty}^{t_o} U_o P(X,V,\kappa,t_o - t)dt \qquad (3)$$

where X, V, and κ are all slowly varying functions of time. In the limit that the parameters are constant, the right hand side of equation (2) can be integrated with respect to t and equation (3) reduces to the familiar stationary solution $U_s(X)$

$$U_s(X) = U_o \, e^{\frac{-VX}{\kappa}} \tag{4}$$

The effect of time variations can be understood by examining the behavior of P (t) as illustrated in Fig. 1 for two different values of κ. P is plotted as a function of the time in the past at which a particle seen now (at $t = t_o$) entered the modulating region. Note that the most probably time delay is about 34 days for $\kappa = 2 \times 10^{21}$ cm^2/sec and 40 days for $\kappa = 1.6 \times 10^{21}$ cm^2/sec. Thus a 20% difference in κ corresponds to about a 17% difference in time delay for the example shown. The important point is that if the interplanetary medium characteristics (κ,V,X) are changing in time, even slowly, particles of different κ are sampling these characteristics at different times. Therefore the observed intensity over a range of energies (and κ's) at a particular time corresponds to a set of different average modulating parameters occuring over a range of times in the past. This will result in a "phase lag" which depends on κ(R) (and X and V).

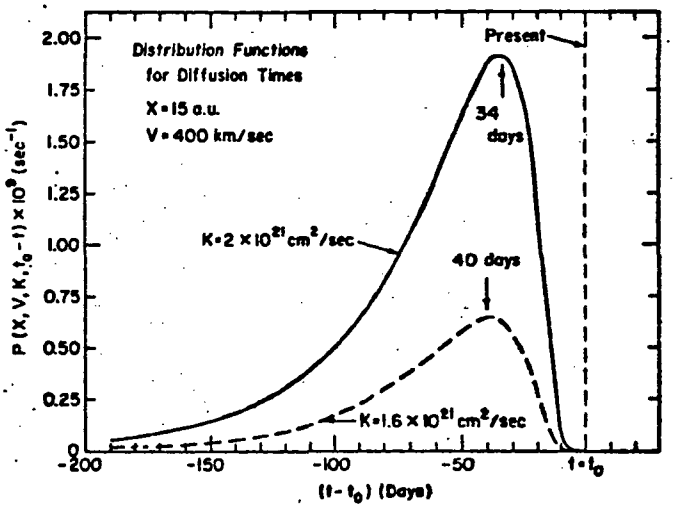

Fig. 1. The distribution of delay times between the detection of a particle at $t = t_o$ and its having entered the modulating region at some prior time t. The area under each curve is equal to $e^{-VX/\kappa}$ and the most probable time shifts to longer times for smaller κ.

The effect is best represented formally in terms of the average time delay τ which is somewhat longer than the most probable delay time indicated in Fig. 1. The average time is defined as follows:

$$\tau = \frac{\int_o^\infty t \, P(t) dt}{\int_o^\infty P(t) dt} \tag{5}$$

It should be noted that changes in τ produced by changes in P with time are second order effects and are to be neglected in evaluating equation (5). It is shown in Appendix I that to first order the solution of equation (3) under slowly varying conditions at a given time $t = t_o$ is given by

$$U(X,t_o) \overset{\sim}{=} U_s[X, t_o - \tau(\kappa)] \tag{6}$$

At high energies $\kappa(R)$ becomes very large and $\tau(T)$ becomes small and the expected intensity is equivalent to the stationary solution. Equation 6 therefore shows that time dependent diffusion provides a mechanism for producing a phase lag at low energies with respect to that at high energies, i.e. a "hysteresis effect".

3. Evaluation of τ and Comparison with Observations. Equation (5) which can be written explicitly as:

$$\tau(X,V,\kappa) = \frac{Xe^{\frac{VX}{\kappa}}}{(4\pi\kappa)^{\frac{1}{2}}} \int_0^\infty t^{-\frac{1}{2}} e^{\frac{-(vt + X)^2}{4\kappa t}} dt \qquad (7)$$

where the normalizing denominator in equation 5 has been explicitly written as $e^{VX/\kappa}$. Again for simplicity we consider only the limiting cases of large and small κ. In the case of large κ (i.e. $VX/\kappa << 4$) the convection term in the exponent of the integral in equation 7 can be neglected in the integration yielding

$$\tau(X,\kappa) \simeq \frac{X^2}{2\kappa} \qquad (8)$$

which is equivalent to the diffusive propagation time in a one dimensional array of fixed scattering centers. In the limit of small κ ($XV/\kappa >> 4$) the diffusion term in the exponent of the integral in equation 7 is neglected in the integration with the result that

$$\tau(X,V) \simeq \frac{X}{V} \qquad (9)$$

The limiting behavior predicted by equations (8) and (9) can be compared directly with observations to illustrate the concepts of the model.

A detailed study of the rigidity dependence of the magnitude of hysteresis effects for a fixed value of the Deep River neutron intensity has been compiled by Rygg, et al. (1973). These same data also have been analyzed to find the time lags between the proton and helium intensities and the neutron intensities which result in a single valued regression (i.e. a closed loop). The values derived from the observations are listed in Table I along with the corresponding rigidity, velocity and diffusion coefficient κ (calculated from the Mariner IV Interplanetary Magnetic Field Spectra as given by Jokipii and Coleman 1968).

TABLE 1

Observed Hysteresis Phase Lags

	Energy	Rigidity	B	$\kappa_{cal}(cm^2/sec)$	τ(days)
Protons	60MeV	.341GV	.34	1×10^{21}	150 ± 30
	100-250	.600GV	.54	2.6×10^{21}	150 ± 30
	260-720	1.078GV	.754	4×10^{21}	120 ± 45
	>720	>1.368	>.824	>6.2	45 ± 10
Helium	60MeV/nuc	.682	.34	1.7×10^{21}	150 ± 30
	100-150MeV/nuc	1002	.47	2.8×10^{21}	60 ± 15
	200-250MeV/nuc	1376	.59	4.4×10^{21}	45 ± 15
	>260MeV/nuc	>1492	>.62	>.53	40 ± 10

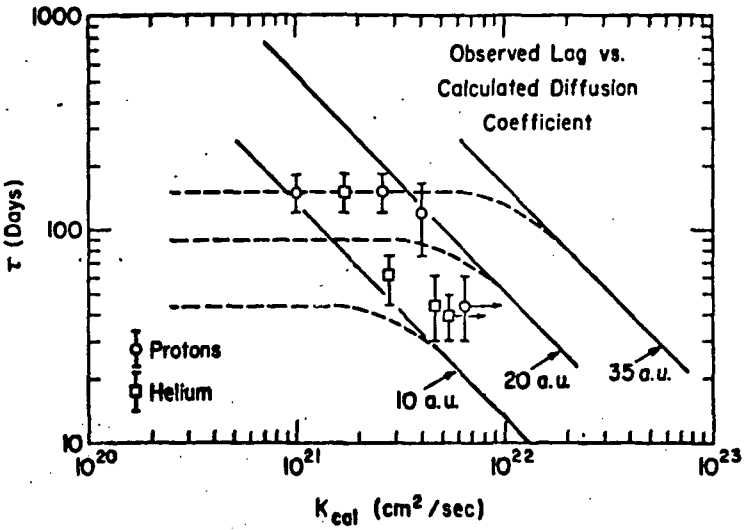

Fig. 2.
Observed delay times for protons and helium nuclei during the 1969-1970 Solar Maximum. The points are plotted at calculated values of κ based on the work of Jokipii and Coleman (1968). The curves indicate the expected dependence of τ on κ for three positions of the modulating boundary under the approximation of the model.

These observations are compared in Fig. 2 with the predictions of the limiting approximations to equation 7 discussed above. The observed time lags are plotted as a function of the corresponding calculated value of κ showing a gradual decrease with increasing κ. The solid straight lines represent the diffusive progagation times (equation 8) in interplanetary regions of 10, 20 and 35 a.u. respectively. The curved dashed lines represent the limiting behavior at small κ (equation 9) for these same regions. The observations are seen to be crudely consistent with the areas bounded by the solid lines for 10 and 20 a.u. However, the approximation for ignoring the convection term in equation 7 is breaking down in the region where the data are plotted. If the upper limit imposed by equation 9 is taken literally (it may in fact be wrong by factor $\sim$2 because of our use of a one dimension model), the largest observed phase lags of up to $\sim$150 days imply a modulating region somewhat larger of $\sim$ X = 35 a.u. Furthermore to be consistent with the model the characteristic diffusion coefficient for the observed particles over the whole region would be somewhat larger than the values plotted here. In particular if the average value of κ for these particles were a factor of $\sim$7 larger, equation 8 would be quite valid and would lead to agreement with the observations in a region of 30-40 a.u. Such a result, modulation in large region with large diffusion coefficient, is consistent with current hysteresis observations and the small gradients currently being reported on Pioneer 10 (McKibben, et al. 1973).

The model presented here provides an explanation of "hysteresis" which does not require that κ be an inseparable function of R, t and V although such behavior may be part of the complete picture. Furthermore, more sophisticated analysis based on these concepts may provide an explanation for the anamolous behavior of the helium spectrum reported recently (Mason, Munoz and Simpson, 1973).

Appendix 1

To determine the effects of slowly varying interplanetary conditions we express the probability density P(t) as

$$P(X,V,\kappa,t) = P_o(t) + \delta P_o(t) + \ldots \qquad A_1)$$

where

$P_o(t) = P(X_o, V_o, \kappa_o, t)$ is $P_o(t)$ evaluated under conditions existing at $t = t_o$ and

$$\delta P_o(t) = \left| \frac{\partial P_o}{\partial X}\frac{\Delta X}{\Delta t_o} + \frac{\partial P_o}{\partial V}\frac{\Delta V}{\Delta t_o} + \frac{\delta P_o}{\partial \kappa}\frac{\Delta \kappa}{\Delta t_o} \right| (t - t_o) \qquad A_2)$$

with $\Delta X/\Delta t_o$, $\Delta V/\Delta t_o$ and $\Delta\kappa/\Delta t_o$ being the slow rates of change in each of these parameters. Under these conditions we can write equation 3 in the text as

$$U(X,t_o) = \int_{-\infty}^{t_o} U_o P_o(t_o - t)\, dt + \int_{-\infty}^{t_o} U_o[t - t_o]\, \frac{\delta P_o}{\delta t_o}\,(t_o = t) + \ldots \qquad A_3)$$

The first term on the righthand side is simply $U_s(X,t_o)$ by definition. We evaluate the second term subject to the condition that $[1/P_o \cdot \delta P_o/\delta t_o]^{-1} >> \tau$ as defined by equation (5). (In the stationary solution the assumption is that $[(1/P)(\delta P/\delta t_o)]^{-1} = \infty$. Here for the first order contribution we simply assume it is very large but not infinite.) Thus we can take this derivative with respect to t_o out of the integral and write the second term of A_3 as

$$\frac{\delta}{\delta t_o}\left| U_o \int_{-\infty}^{t_o} [t - t_o]\, P_o(t_o - t)dt \right| = -\frac{\delta}{\delta t_o}\left| \tau \int_{-\infty}^{t_o} U_o P_o(t_o - t)dt \right| \qquad A_4)$$

where we have used the definition of τ in equation (5). Thus equation A_3 can be rewritten as

$$U(X,t_o) = U_s(X,t_o) - \tau\,\frac{\delta}{\delta t_o}\,[U_s(X,t_o)] + \ldots \simeq U_s(X,t_o - t) \qquad A_5)$$

where we have evaluated $\delta/\delta t_o$ over a time interval τ neglecting changes in τ as second order effects.

Acknowledgements: I am indebted to Dr. Thomas Rygg for several extended discussions of this problem. This work was supported in part by NASA Grants NGR 21-002-066 and NGL 21-002-033.

References

Balasubramanyan, V.K., D.E. Hagge and F.B. McDonald, Can. J. Phys. 46, S887, 1968.
Burger, J.J. and B.N. Schwannenberg, J. Geophys. Res. 78, 292, 1973.
Forbush, S., J. Geophys. Res. 59, 525, 1954.
Kane, S.R., and J.R. Winkler, J. Geophys. Res. 74, 6247, 1969.
Mason, G.L., M.G. Munoz and J.A. Simpson, to be published in Astrophys. Letters.
McKibben, R.B., G.A. Lentz, J.J. O'Gallagher, M. Perkins, J.A. Simpson and A.J. Tuzzolino, Paper 153, this conference, 1973.
Parker, E.N., Interplanetary Dynamical Processes, John Wiley & Sons, NY 1963.
Parker, E.N., Planet. and Space Sci. 13, 9, 1965.
Rygg, T.A., J.J. O'Gallagher and J.A. Earl (to be published 1973).
Schmidt, P.J., J. Geophys. Res. 77, 3295, 1972.
Simpson, J.A., Proc. Conf. Cosmic Radiation in Interplanetary Space (Vatican), 323, 1963.
Simpson, J.A. and J.R. Wang, Astrophys. J. 161, 265, 1970.
Van Hollebeke, M.A., J.R. Wang and F.B. McDonald, J. Geophys. Res. 77, 6881, 1972.

Technical Report #73-132

DIRECT OBSERVATIONS OF THE CHARGE STATES OF LOW ENERGY SOLAR PARTICLES

G. Gloeckler

Department of Physics and Astronomy, University of Maryland
College Park, Maryland (USA) 20742

C.Y. Fan

Physics Department, University of Arizona, Tucson, Arizona (USA) 85721

D. Hovestadt

Max-Planck Institut für Extraterrestrische Physik
8046 Garching (Germany)

The charge states of carbon and oxygen of solar origin have been measured directly in interplanetary space. At 100 keV per nucleon the C^{+5}/C^{+6} and O^{+7}/O^{+8} ratios are 1.8 and 1.6 respectively. We find the abundance ratios of low energy heavy nuclei to He significantly larger than corresponding photospheric values: The enhancement of O/He is 35 and both Si/He and Fe/He are overabundant by a factor of 100. To explain these observations we propose a mechanism which first preferentially accelerates heavy ions and is followed by either storage of these ions in the coronal regions or strong adiabatic decleration.

1. Introduction. Chemical composition measurements of solar flare particles above 10 MeV per nucleon, pioneered by the Goddard Emulsion Group (Fichtel and Guss, 1961; Biswas and Fichtel, 1965), have been extended in recent years to very low energies using dielectric track recording devices (Fleischer and Hart 1973; Braddy et al. 1973; Crawford et al. 1972). The most striking feature of these low energy (<10 MeV per nucleon) observations has been the enhancement of the ratios of heavy to light nuclei over corresponding photospheric ratios in contrast to results of the Goddard group at higher energies (>10 MeV per nucleon), which showed that the solar particle composition reflected photospheric abundances (Bertsch et al. 1973). Mogro-Campero and Simpson (1972) find that 5-60 MeV per nucleon solar cosmic rays also show a heavy particle enrichment which increases with atomic number and varies from flare to flare. To explain the increasing enhancement of heavy nuclei both with decreasing energy and increasing charge various acceleration models have been proposed, all of which require an establishment of charge state equilibrium for ions in the acceleration process (Ginzburg and Syrovatskii 1964, and references therein; Ramadurai 1971; Cartwright and Mogro-Campero 1972). Direct measurements of the charge state of low energy ions are therefore clearly important in order to check the validity of these models.

In this paper we present our preliminary results on low energy charged particles observed during a small energetic particle event on October 17-18, 1972. Our measurements provide the first direct evidence for partially stripped carbon and oxygen at 100 keV per nucleon and extend heavy ion measurements down to 50 keV per nucleon.

2. Instrument Description. The data have been obtained using the University of Maryland Electrostatic Deflection Analyzer (Fan et al. 1971) on board the IMP 7 (Explorer 47) satellite which was launched September 22, 1972 into

a nearly circular, 240 000 km apogee orbit. Our method of particle identification is based on the fact that the amount of deflection, d, of a non-relativistic ion with an effective charge Z^* and kinetic energy T in a known electrostatic field is given by $d = gZ^*/T$. The constant g is determined by the geometry and voltage of the deflection system.

In Fig. 1 we show the cross sectional sideview of the sensor designed to measure particles in the energy range 50 to 1000 keV per nucleon. The collimator defines the incoming direction of the ion, three separate electric field regions (two low field and one high field) provide the necessary deflection, and ten rectangular solid state detectors are used to measure the energy T and deflection d. A plastic scintillator cup is used to reduce penetrating charged particle background.

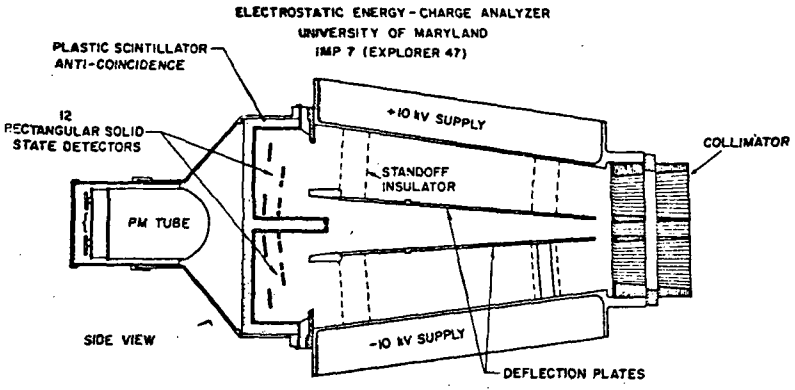

Fig. 1. Cross sectional side view of the Electrostatic Energy-Charge Analyzer. The geometrical factor for each of the low field deflection regions is 3 mm^2 sr. For the high field region it is 1.8 mm^2 sr.

Fig. 2 illustrates the charge resolution of the instrument. The deflection vs. energy lines for each given charge Z^* are broadened to reflect the energy and geometrical resolutions of the detector system. Dashed horizontal lines correspond to boundaries of sensitive areas of given solid state detectors and define the energy window for each detector. The electronics associated with the sensor identify the triggered detector and record the pulse height of the signal proportional to the total energy of the particle at a maximum rate of 0.9 events/sec. In addition, sectored counting rates corresponding to the absolute particle fluxes in selected and fixed energy per charge windows are transmitted once every 5 sec.

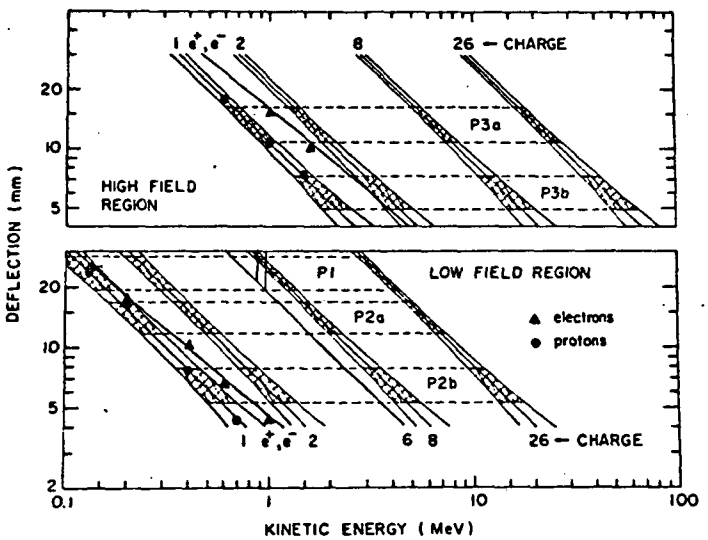

Fig. 2. Deflection vs. energy curves for particles having charge states 1, 2, 6, 8 and 26 in the high and low field deflection regions of the instrument. Proton and electron calibrations were used to derive these curves. Shaded areas show the allowed energy ranges in each detector and indicate the charge resolution of the sensor. The energy ranges are fixed by the position and geometry of the detectors, and the voltage of the deflection system.

The pulse height information is essential for identification of the charge state of an ion. A projection of the shaded portions of deflection vs. energy curve in Fig. 2 for a given detector on the energy axis shows

that one can easily resolve charge states 1, 2, 5-8, and 20-26 over the entire energy range of each detector. In addition, by making reasonable assumptions concerning relative abundances of heavy nuclei, it is possible to identify adjacent charge states in the 5-8 group in more restricted energy intervals.

3. Results. Solar particles observed near earth on October 17 and 18 were probably produced by a subflare on the eastern limb of the sun (S06, E66) beginning at 0830UT on October 16, 1972. A sudden commencement (1800 UT October 18) and Forbush decrease (2400UT October 18) accompanied this event. The 10 minute averaged counting rate proportional to the flux of 125-160 keV protons is shown in Fig. 3 and illustrates the complex structure of this event. The initial increase above background occurs at about 0200UT on October 17, some 17 hours after the onset of the parent flare, and is followed by two more prominent increases at 2000UT, October 17 and 1100UT, October 18. In the insert we show that the satellite was outside the bow-shock region during the major portion of the event. Hourly averages of the proton to helium ratio computed at equal velocities (120 keV per nucleon) were found to remain constant at about 40 throughout the entire event. Time averaged abundances ratios should therefore be computed on an equal energy per nucleon basis.

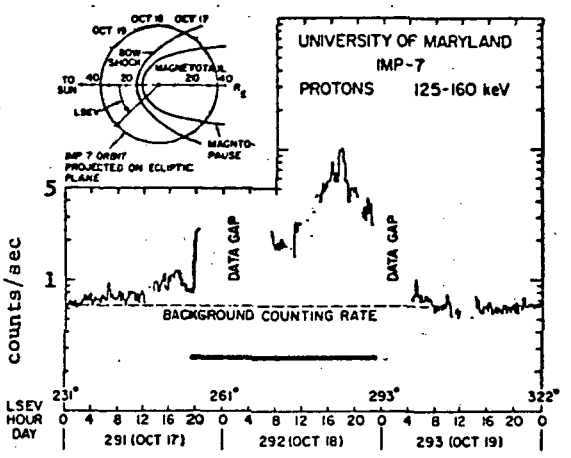

Fig. 3. Time profile for 125-160 keV protons for the three day period October 17-19, 1972. The background rate of 0.65 counts/sec is most likely due to the sensitivity of solid state detectors to γ rays generated in the spacecraft. The peak rate of 10 counts/sec corresponds to a differential flux of 1.3×10^4 protons/(cm^2 sec sr MeV).

Our results on spectra and abundances of particles are based on data averaged over the 30 hour time period shown by the solid bar in Fig. 3. For reference we present in Fig. 4 the time averaged proton and helium spectra. We note that these are best represented by a dependence on rigidity, P, of the form $dJ/dP = J_o \exp(-P/P_o)$ with different characteristic rigidities P_o. Since the proton spectrum is steeper than the helium spectrum the p/α ratio depends on energy and goes from 14 at 20 MV to 2 at 50 MV.

The spectra of heavy particles appear in Fig. 5. Assuming the nuclei to be fully stripped (Braddy, et al. 1973) we compute spectra for the CNO, Si and Fe group nuclei and show these, plotted as a function of kinetic energy per nucleon, along with the helium spectrum in Fig. 5(a). We find that the abundances of Fe and Si are about equal within errors of the measurement and that the Si/He and Fe/He ratios at 100 keV per nucleon are about 0.025, or larger by a factor of 100 than the corresponding solar photospheric values. Fig. 5(b) gives two point carbon and oxygen spectra computed under the assumption that these nuclei are fully stripped and that small amounts of B, N, and Ne are present. The C/O value obtained is about 2 to 3 which is much higher than the usual value of 0.5 for solar cosmic rays (Teegarden et al. 1973). Furthermore, using the dE/dx vs. E telescope ULET (Hovestadt and Vollmer 1971) flown on the same spacecraft we find for the identical time period the C/O ratio at 500 keV per nucleon to be 0.5±0.1.

Fig. 5(c) shows the spectra of partially stripped nuclei. Retaining the assumption that very little Be, B, N and Ne is present we have taken all $Z^* = 5$ to be C^{+5} and all $Z^* = 8$ to be O^{+8}. It is then possible to estimate the abundances of C^{+6} and O^{+7}. The $(C^{+5} + C^{+6})/(O^{+7} + O^{+8})$ ratio now becomes 0.8 and is in reasonable agreement with measurements at 500 keV per nucleon. In Table I we list our results on abundances at 100 keV per nucleon along with previously published values at higher energies and photospheric abundances. A systematic increase in the enhancement of heavy nuclei is evident both with decreasing energy and increasing atomic number of the particles. For example, 100 keV per nucleon solar flare O, Si and Fe nuclei are overabundant relative to the solar photosphere by factors of 35, 70 and 100 respectively.

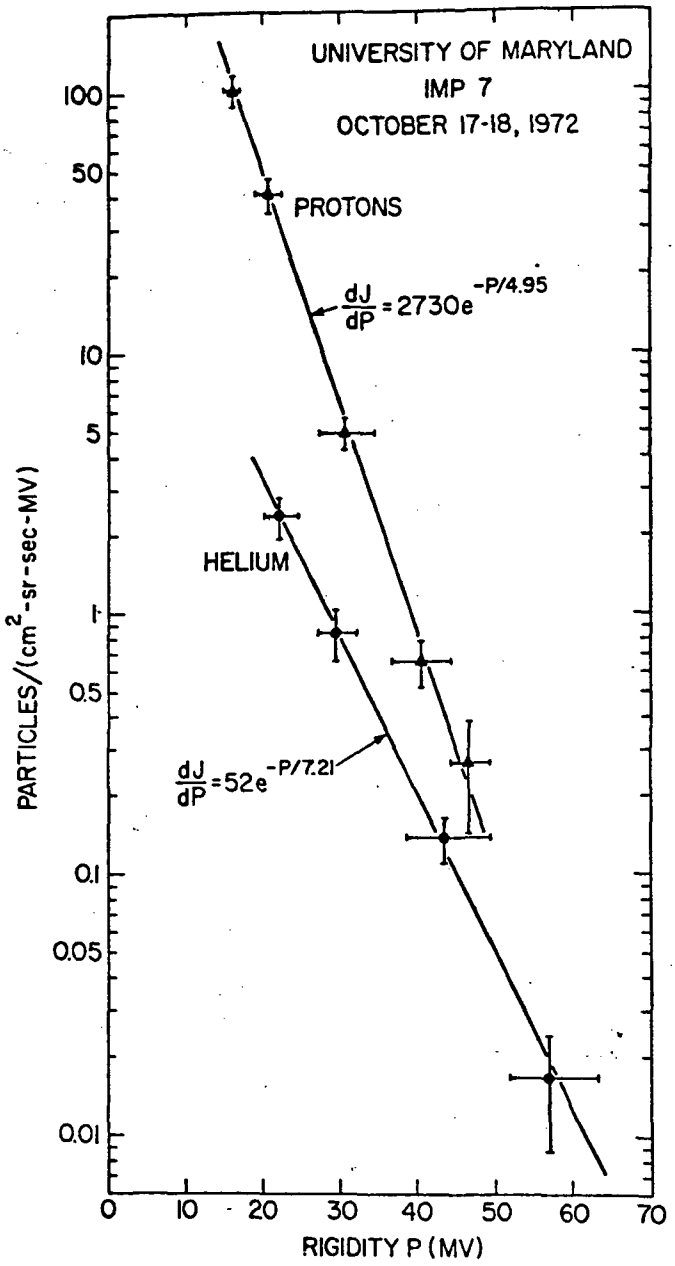

Fig. 4. Time averaged proton and helium differential rigidity spectra. To obtain these spectra we have corrected the pulse height distributions for background and used the fixed energy windows for each detector to compute the flux.

4. Discussion. The enrichment of heavy low energy nuclei in solar cosmic rays relative to solar photospheric abundances, and the presence of significant amounts of partially stripped nuclei are indicative of the acceleration process and the physical conditions of the medium where the acceleration occurred. We can suggest the following model to provide a qualitative explanation for these observations.

To produce an enhancement of heavy nuclei we require statistical acceleration in regions of sufficient neutral hydrogen density for charge equilibrium to be established (Ginzburg and Syrovatskii, 1964; Ramadurai 1971). Acceleration of this type can account for the observed energy dependence of the heavy particle enrichment. Under these conditions, the charge state of the accelerated particles will depend on their energy. For example, the equilibrium charge states of carbon and oxygen at 100 keV per nucleon are found to be 2.5 and 2.9 respectively. Our measurements on the other hand, indicate much higher values, specifically 5.4 for carbon and 7.4 for oxygen. To account for this discrepancy we propose two alternatives.

(1) Accelerated ions traverse hot coronal regions where the probability for electron pickup is vanishingly small, and are stripped of most of their remaining electrons. Given an integrated column density of about $3 \times 10^{18}/cm^2$ and a cross section for stripping of a K-electron of the order of 10^{-21} cm^2, we conclude that the ions must have been confined within the coronal region for about an hour before escape.

(2) After acceleration and escape from the sun, the particles are adiabatically decelerated (Jokipii, 1973). In this case, the measured charge states are the equilibrum charge states of particles at much higher energies. Our measurements of the abundance ratios C^{+5}/C^{+6} and O^{+7}/O^{+8} would imply energy losses of the order of a factor of ten.

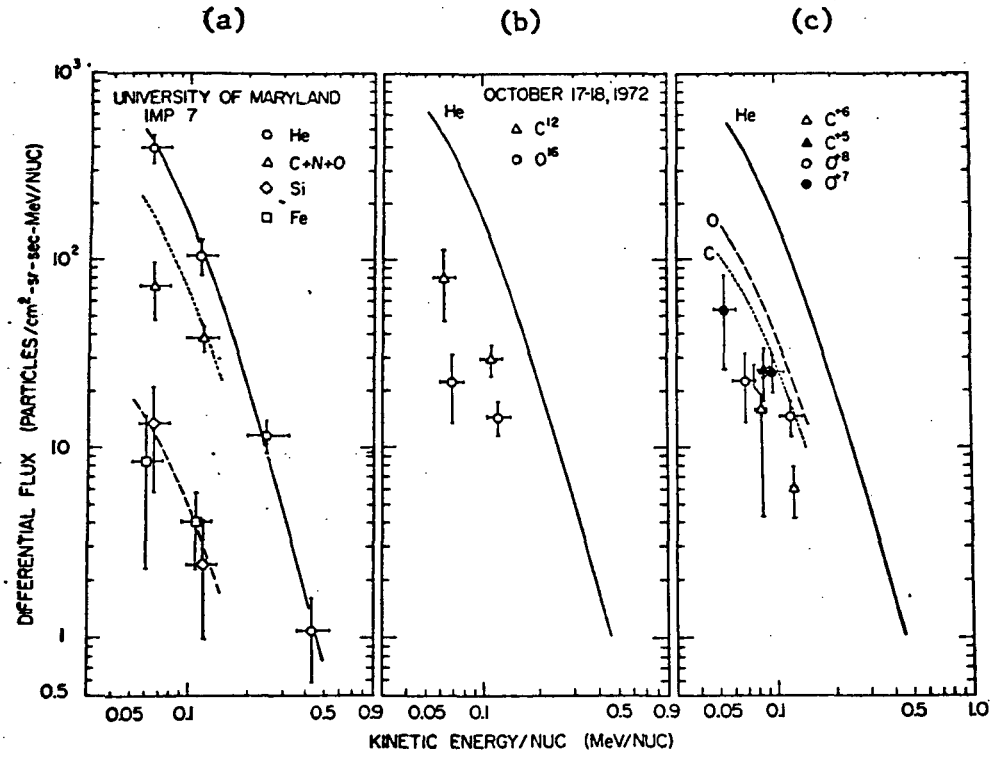

Fig. 5. The time averaged differential energy spectra for helium and heavy particles. Data have been corrected for energy defects in the solid state detector and for background measured independently for each detector with the deflection voltages commanded off. The dashed and dotted curves represent a scaled helium spectrum and are drawn for reference only. (a) Spectra of CNO, Si and Fe group nuclei assuming full stripping. (b) Carbon and Oxygen spectra. (c) Spectra of partially stripped nuclei.

Table 1. Abundance Ratios for Solar Flare Particles at Different Energies

Abundance Ratio	Solar Flare Particles			Photosphere[d]
	0.1 MeV/nuc.[a]	1.5 MeV/nuc.[b]	14-50 MeV/nuc.[c]	
C^{+5}/C^{+6}	1.8			
O^{+7}/O^{+8}	1.6			
O/He	0.25	0.15	0.025	0.0068
Si/He	0.025	0.012	0.0025	0.00035
Fe/He	0.025	0.018	0.0007	0.00025

[a]Present work.
[b]Data compiled by Lanzerotti et al. 1972.
[c]Teegarden et al. 1973.
[d]Hange and Engvold 1970; Withbroe 1971.

The limited amount of data we have at present does not allow us to decide which of the two alternatives corresponds to actual conditions. More extensive observations of low energy ions will be required before decisive information about particle acceleration and their subsequent propagation to earth is obtained.

Acknowledgements. This research was supported by the National Aeronautics and Space Administration under contract NAS5-11063, and grant NGR 21-002-224. Of the many individuals in the Department of Physics and Astronomy of the University of Maryland who have contributed to the success of this experiment we are particularly grateful to E. Tums for the electronic design, fabrication and testing, J. Cain for the mechanical design and fabrication of the instrument and collimator, and to R. Sciambi for his help in the testing and calibration of the instrument. We thank J. Gigante and R. Lundgren for designing, fabricating and testing the rectangular solid state detectors, and J. Dalton for developing our computer programs. We especially acknowledge the excellent cooperation of the IMP Project Staff, in particular M.A. Davis, and their efforts in integrating our experiment with the IMP 7 spacecraft and its launching.

References

Bertsch, D.L., Fichtel, C.E., Pellerin, C.J., and Reames, D.V. 1973, Ap. J. 180, 583.
Biswas, S., and Fichtel, C.E. 1965, Space Sci. Rev. 4, 709.
Braddy, D., Chan, J., and Price, P.B. 1973, Phys. Rev. Letters, 30, 669.
Cartwright, B.G., and Mogro-Campero, A. 1972, Ap. J. (Letters), 177, L43.
Crawford, H.J., Price, P.B., and Sullivan, J.D. 1972, Ap. J. (Letters), 175, L149.
Fan, C.Y., Gloeckler, G., and Tums, E. 1971, 12th International Conference on Cosmic Rays (University of Tasmania), Vol. 4, p. 1602.
Fichtel, C.E., and Guss, D.E. 1961, Phys. Rev. Letters, 6, 495.
Fleischer, R. L., and Hart, H.R. Jr. 1973, Phys. Rev. Letters, 30, 31.
Ginzburg, V.L., and Syrovatskii, S.I. 1964, The Origin of Cosmic Rays (Oxford: Pergamon Press), p. 162.
Hange, O., and Engvold, O. 1970, Inst. of Theor. Astrophys. Report No. 31, Blindern, Oslo, Norway.
Hovestadt, D., and Vollmer, O. 1971, 12th International Conference on Cosmic Rays (University of Tasmania), Vol. 4, p. 1608.
Jokipii, J.R. 1973, private communication.
Lanzerotti, L.J., Maclennan, C.G., and Graedel, T.E. 1972, Ap. J. (Letters), 173, L39.
Mogro-Campero, A., and Simpson, J.A. 1972, Ap. J. (Letters), 177, L37.
Ramadurai, S. 1971, 12th International Conference on Cosmic Rays (University of Tasmania), Vol. 1, p. 385.
Teegarden, B.J., Von Rosenvinge, T.T., and McDonald, F.B. 1973, Ap. J., 180, 571.
Withbroe, G.L. 1971, U.S. Dept. Commerce, NBS Spec. Report Publ. No. 353, p. 121.

Technical Report #73-133

COHERENT PROPAGATION OF CHARGED PARTICLE BUNCHES IN RANDOM MAGNETIC FIELDS

James A. Earl

Department of Physics and Astronomy, University of Maryland
College Park, Maryland (USA) 20742

When the distribution function for energetic particles moving in interplanetary space is expressed in terms of eigenfunctions of an operator which describes pitch angle scattering by random magnetic fields, the familiar phenomenon of diffusion is the dominant solution of the transport equations provided that the spectrum of magnetic fluctuations is not too steep. However, if this condition is not satisfied, the dominant solution of the same equations is a new mode of transport in which density inhomogeneities propagate coherently along the guiding field with a characteristic velocity equal to half the particle speed. The most striking manifestation of this phenomenon is the observed "scatter free" propagation of solar flare electrons below 1 MeV.

1. Introduction. For many years, it has been virtually taken for granted that cosmic ray propagation is fundamentally diffusive in nature. In early papers, the scattering centers responsible for diffusion were visualized as discrete magnetized clouds. However, in the physically more plausible configuration of random fields superimposed upon a smooth guiding field, diffusive transport, characterized by a finite diffusion coefficient, has also been established as a fundamental mode provided that small scale fluctuations among the random perturbing fields are sufficiently intense (Jokipii, 1966; Hasselman and Wibberenz, 1970; Earl, 1973). More specifically, if the spectrum of magnetic energy density vs. wavenumber k which characterizes the perpendicular irregularities is a power law $P(k) \propto k^{-q}$ with spectral index q, then diffusion occurs when $q < 2$. This paper describes a novel mode of particle transport in which, for $q \geq 2$, density inhomogeneities propagate in a wavelike fashion with very little dispersion. Because this behavior is qualitatively different from diffusion, the new mode will be designated as "coherent". Since a complete treatment of these effects is available in a longer report with the same title as this one (U. of MD., TR #73-098), only the most basic features of the coherent mode will be presented here with emphasis on physical interpretations rather than on mathematical proofs.

2. Transport Equations. In the present one-dimensional case, the Boltzmann equation can be written as

$$\frac{\partial f}{\partial t} + \mu V \frac{\partial f}{\partial z} - \frac{1}{2} \frac{\partial}{\partial \mu} \frac{\langle \Delta\mu^2 \rangle}{\Delta t} \frac{\partial f}{\partial \mu} = 0 \qquad (1)$$

where μ is the cosine of the pitch angle relative to the guiding field, t is time, V is particle velocity, z is distance along the mean field, and f is particle density in phase space. (For momentum p, this quantity is proportional to cosmic ray flux, $J = f/p^2$.) The last term in Eq. 1 describes

pitch angle scattering as characterized by a Fokker-Planck coefficient given by Jokipii (1966) in the form,

$$\frac{\langle \Delta\mu^2 \rangle}{\Delta t} = A\,(1 - \mu^2)\,|\mu|^{q-1} \qquad (2)$$

where q is the spectral index discussed earlier and A is a parameter which depends on the r.m.s. intensity of the random fields and upon particle momentum and velocity. The key to understanding Eq. 1 is to recognize that the scattering operator is such that Sturm Liouville theory is applicable. This ensures that there exist eigenfunctions R_κ and relaxation times τ_κ which are defined by

$$\frac{\partial}{\partial\mu}\frac{\langle \Delta\mu^2 \rangle}{\Delta t}\frac{\partial R_\kappa}{\partial\mu} + \frac{2}{\tau_\kappa} R_\kappa = 0 \qquad (3)$$

and that the distribution function can be expressed as an eigenfunction series $f = \Sigma f_\kappa R_\kappa$ in which the coefficients f_κ decrease in magnitude rapidly with κ so that only the first few terms are needed to represent f quite accurately. Because the functions R_κ form an orthogonal set, it is easy to derive the following set of coupled differential equations for the coefficients:

$$\frac{\partial f_0}{\partial t} = -V_{01}\frac{\partial f1}{\partial z} - V_{03}\frac{\partial f_3}{\partial z} \quad (4) \qquad \frac{\partial f_1}{\partial t} + \frac{f_1}{\tau_1} = -V_{01}\frac{\partial f_0}{\partial z} - V_{12}\frac{\partial f2}{\partial z} \quad (5)$$

$$\frac{\partial f_2}{\partial t} + \frac{f_2}{\tau_2} = -V_{12}\frac{\partial f_1}{\partial z} - V_{23}\frac{\partial f3}{\partial z} \quad (6) \qquad \frac{\partial f_3}{\partial t} + \frac{f_3}{\tau_3} = -V_{03}\frac{\partial f_0}{\partial z} - V_{23}\frac{\partial f_2}{\partial z} \quad (7)$$

where V_{01}, V_{03}, V_{12} and V_{23} are characteristic velocities defined by integrals which would take too much space to give here but which are exactly analogous to quantum mechanical matrix elements. The coefficient f_0 of the isotropic eigenfunction R_0 = const. is proportional to the spatial density U while the odd anisotropic components R_1, R_3, ... give rise to a streaming flux S whose gradient is equal to the time rate of change of density. In diffusion, only the two lowest order components f_0 and f_1 are important, but, in coherent transport, the components f_2 and f_3 also play a significant role.

To make clear the difference between coherent and diffusive regimes, it is worth considering, for each case, how scattering causes the first order anisotropy R_1 to change with time. In Fig. 1a, the Fokker-Planck coefficient defined for $q < 2$ by Eq. 2 (solid curve) dips to zero in the cusp at $\mu = 0$, but the slope of R_1 at this point is very steep. (See Fig. 1b.) Consequently, a large derivative acts in the scattering operator to compensate for weak scattering so as to produce the same fractional rate of change at $\mu = 0$ as everywhere else. Thus, according to Eq. 3, an anisotropy proportional to R_1 will decay exponentially with no change in shape at a rate characterized by the relaxation time τ_1. As will be indicated later, this rapid decay of the first anisotropy is closely related to diffusion. In the coherent regime, $q \geq 2$, the dashed curve describing $(\langle \Delta\mu^2 \rangle/\Delta t)$ not only has zero

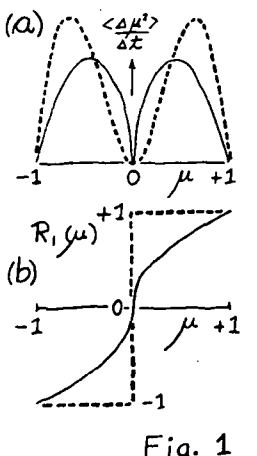

Fig. 1

value but also has zero slope at the origin. This means, in effect, that weak scattering occurs not just at a single point but over a finite region. Consequently, the compensation discussed above does not occur and the eigenfunction R_1 is the step function shown as a dashed curve in Fig. 1b. Moreover, the first relaxation time τ_1 is infinite because the derivative of the step function is zero in regions where the Fokker-Planck coefficient is large, while near the origin where the derivative is large, the coefficient vanishes. For $q < 2$, the situation is analogous to quantum mechanical tunneling in that particles are able to pass through the region of weak scattering at $\mu = 0$ to allow a first order anisotropy to relax. For $q \geq 2$, this effect is inhibited so that an anisotropy proportional to the step function is stable. It is this persistence of anisotropy that gives rise to coherent effects.

3. Diffusion. In standard works on transport theory (Weinberg and Wigner, 1958, p. 231), the diffusion approximation is obtained by neglecting the derivative $(\partial f_1/\partial t)$ as well as coefficients of higher order than f_1. Thus, according to Eq. 5, the f_1 component reaches a secular equilibrium, $f_1 = -\tau_1 V_{01}(\partial f_o/\partial z)$ which can be substituted into Eq. 4 to give the diffusion equation

$$\frac{\partial f_o}{\partial t} = \tau_1 (V_{01})^2 \frac{\partial^2 f_o}{\partial z^2} = D \frac{\partial^2 f_o}{\partial z^2} \tag{8}$$

Evidently the diffusion coefficient $D = \tau_1 (V_{01})^2$ is well defined when τ_1 is finite but it becomes infinite in the coherent regime. The solution of Eq. 8 for impulsive injection at $t = 0$ and $z = 0$ of a localized bunch of particles is the familiar Green's function for diffusion

$$f_o = [F_o/(4\pi Dt)^{\frac{1}{2}}] \exp\{-z^2/4Dt\} \tag{9}$$

where F_o is a measure of the total number of particles injected.

4. The Coherent Regime. When $q \geq 2$, the eigenfunctions R_2 and R_3 are not only important but also they are "degenerate" in the sense that their eigenvalues are equal so that $\tau_2 = \tau_3$. Furthermore, $V_{03} = V_{12}$ and $\tau_1 = \infty$. Under these circumstances, the symmetry of Eqs. 4 - 6 is such that the solutions must meet one of the following two conditions:

$$f_o^+ = + f_1^+;\ f_2^+ = + f_3^+ \qquad \text{or} \quad f_o^- = - f_1^-;\ f_2^- = - f_3^- \tag{10}$$

In the spirit of the diffusion approximation discussed above, the spatial and temporal derivatives of f_2 and f_3 can be neglected so that Eqs. 4 and 6 combine to give an equation for f_o

$$\left[\frac{\partial}{\partial t} + V_{01} \frac{\partial}{\partial z}\right] f_o^+ = \tau_3 (V_{03})^2 \frac{\partial^2 f_o^+}{\partial z^2} \tag{11}$$

The transformation $y = z - V_{01}t$ reduces this to

$$\frac{\partial f_o}{\partial t} = \tau_3 (V_{03})^2 \frac{\partial^2 f_o^+}{\partial y^2} = D_* \frac{\partial^2 f_o^+}{\partial y^2} \tag{12}$$

which is of the same form as Eq. 8. Consequently, the solution of Eqs. 11 and 12 corresponding to impulsive injection can immediately be written by analogy with Eq. 9 as

$$f_o^+ = [F_o/(16\pi D_* t)^{\frac{1}{2}}] \exp\{-(z - V_{01}t)^2/4D_* t)\} \qquad (13)$$

where the diffusion coefficient has been replaced by a parameter $D_* = \tau_3(V_{03})^2$ that I call the coefficient of dispersion. In Eq. 13, the diffusive Gaussian of Eq. 9 centered at the stationary point $z = 0$ has been replaced by a moving coherent Gaussian centered at $z - V_{01}t$. For isotropic injection, this localized pulse moving in the $+z$ direction with velocity V_{01} is accompanied by a symmetrical pulse f^- moving in the $-z$ direction. The latter disturbance satisfies the second condition of Eq. 10.

The summation, implied by Eq. 10, of an isotropic component and a step function of equal amplitude gives for f^+ a distribution function which is constant for $\mu > 0$ and zero for $\mu < 0$. (This form is slightly modified by f_2 and f_3 but these components are small compared to f_o and f_1.) This describes a bunch of particles with velocities isotropically distributed over the forward hemisphere with no particles moving backward. The component f^- represents a similar group moving in the opposite direction with velocities in the other hemisphere. These bunches move coherently because the velocity vector of an individual particle wanders randomly over one hemisphere giving an average component along the z axis equal to that of other particles in the group. This speed is $V_{01} = (V/2)$. The steady increase of the width of the coherent disturbances, characterized in Eq. 13 by the dispersion coefficient D_*, results from statistical fluctuations in this averaging of directed random velocities in much the same way that ordinary diffusion results from fluctuations in the averaging of nearly isotropic random velocities.

To summarize, Fig. 2a shows schematically for the diffusive regime the profile of density vs distance z after the injection of a localized pulse at $z = 0$. Here, the narrow spikes shown moving outward with velocities $\pm V_{01}$ on each side of the Gaussian arise when the time derivative $(\partial f_1/\partial t)$ is retained in a treatment similar to the simplified calculation that led to Eq. 8 (Axford, 1965). The number of particles contained in these spikes decreases rapidly leaving the slowly evolving diffusive Gaussian as the dominant contribution. In the coherent regime depicted in Fig. 2b, the density in the coherent Gaussians decreases as they spread out, but the total number of particles in each is constant, and the diffusive Gaussian is completely absent. The qualitative similarity between the coherent disturbances and the spikes of the diffusive regime suggests that, in the case where τ_1 is finite but very large, a useful description can be obtained by simply substituting coherent Gaussians (Eq. 13) for the localized spikes. In this mixed regime, shown in Fig. 2c, the number of particles in the coherent pulses decreases as particles are scattered out of them into the diffusive profile. The mixed regime is of practical

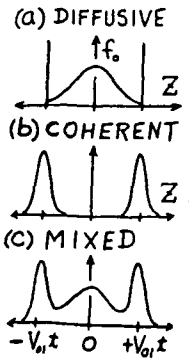

Fig. 2

importance in interplanetary space where direct measurements of an exponent q slightly less than 2 (Sari and Ness, 1969) imply such a large value of τ_1 that coherent effects should be very significant. Moreover, recent theoretical work (Klimas and Sandri, 1972; Kaiser, Jones and Birmingham, 1973) suggests that τ_1 may be large but finite even for $q > 2$. In this case, coherent effects would be very prominent in the mixed regime, but purely coherent transport would not occur.

5. Comparison with Solar Particle Observations. Within the present limitations on length, it is not possible to present and discuss the explicit formulas which relate the parameters appearing above to the power spectrum of interplanetary magnetic fluctuations. However, an implication of these relationships is indicated in Fig. 3 which shows a calculated profile of the intensity of 38 KeV electrons at earth vs. time after injection at the sun. A magnetic power spectrum typical of those actually observed in space was assumed. In the mixed regime occuring here, the coherent pulse is followed by a slowly decaying tail which is, in essence, a diffusive effect. The fact that this profile corresponds in every detail to the phenomenon designated by Lin (1970) as "scatter free" propagation of solar flare electrons makes it clear that the theory explains his observations. However, his terminology seems inappropriate now because it is the existence of scattering within the forward hemisphere that ensures that all electrons have nearly the same average velocity parallel to the field and thus makes possible the propagation of coherent groups.

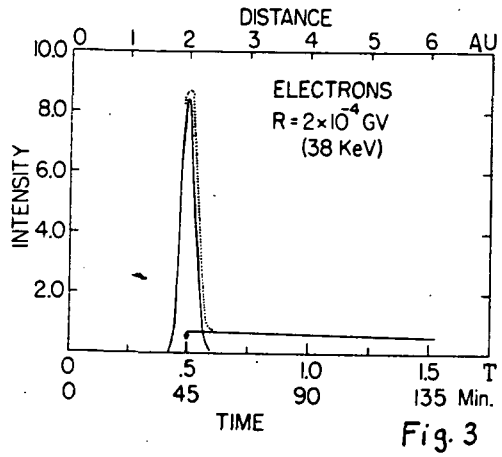

Fig. 3

Coherent propagation offers a convincing explanation for several other poorly understood aspects of solar particle behavior. These include, for example, the initial field-aligned anisotropy of solar particles recorded by neutron monitors (McCracken, 1962) and the double peaked profiles recorded in many events (Fichtel and McDonald, 1967, Fig. 1). To demonstrate that coherent effects are not restricted to low rigidity electrons, Fig. 4 shows how a Gaussian given by Eq. 13 provides a good fit to a flare profile observed by McCracken, Rao and Bukata (1967, Fig. 22) while their detector of 7.5 to 45 MeV protons was pointed toward the sun. The extreme anisotropy predicted above for the coherent pulse explains why the antisun intensity was relatively small. The diffusive tail observed after 0045UT, which is similar to that in Fig. 3, is also predicted.

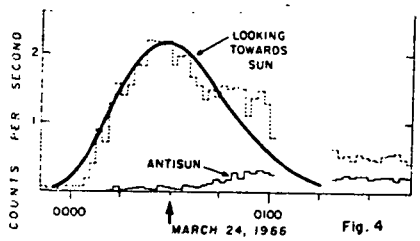

Fig. 4

These interpretations demonstrate that coherent effects exist. However, the real significance of this new understanding of solar phenomena

is to suggest that coherent propagation may also play an important role elsewhere in astrophysics.

Acknowledgements. This research was supported by the National Aeronautics and Space Administration under grant NGR 21-002-066. A useful conversation with R.P. Lin is also acknowledged.

References

Axford, W.I., 1965, Planet. and Space Sci., 13, 1301.
Earl, J.A., 1973, Ap. J., 180, 227.
Hasselmann, K., and Wibberenz, G., 1970, Ap. J., 162, 1049.
Jokipii, J.R., 1966, Ap. J., 146, 480.
Kaiser, T.B., Jones, F.C., and Birmingham, T.J., 1973, Ap. J., 180, 239.
Klimas, A.J., and Sandri, G., 1971, Ap. J., 169, 41.
Lin, R.P., 1970, J. Geophys. Res., 75, 2583.
McCracken, K.G., 1962, J. Geophys. Res., 67, 435.
McCracken, K.G., et. al., 1967, J. Geophys. Res., 72, 4293.
Sari, J.W., and Ness, N.F., 1969, Solar Phys., 8, 155.
Weinberg, A.M., and Wigner, E.P., 1958, The Physical Theory of Neutron Chain Reactors (Chicago, University of Chicago Press).

Technical Report #73-134

BALLOON OBSERVATIONS OF RAPID VARIATIONS IN SOLAR PARTICLE FLUX DURING JULY 1972

Lawrence E. Bagg, James A. Earl, and Janet G. Luhmann

Department of Physics and Astronomy, University of Maryland
College Park, Maryland (USA) 20742

Solar energetic particles were observed with excellent time resolution with the aid of a large hodoscope flown on a balloon. This paper reports on a transient increase in the intensity of solar protons which can be interpreted in considerable detail as evidence for the coherent propagation of particles injected by a west limb flare occurring at 1025UT on July 22, 1972.

1. Introduction. Balloons provide a combination of payload lifting capability and exposure duration that opens up new possibilities for investigating rapid temporal variations of primary cosmic ray intensity. This paper describes an experiment, designed to exploit these possibilities, which employs a detector whose geometric factor is large enough to reveal changes on a scale of minutes in the quiet time flux of 100 to 400 MeV protons. On the one hand, payload weight limitations rule out comparable satellite instruments, while, on the other hand, this region of the primary spectrum is completely inaccessible to large sea level detectors. Moreover, the balloon platform offers the advantage over satellites that intrinsic temporal variations are not obscured by rapid changes resulting from orbital motion through the spatial structure associated with geomagnetic cutoffs.

Recent theoretical work has stimulated interest in "cosmic-ray scintillations" which are broad band intensity fluctuations arising, in much the same way as optical and radio scintillations, from random inhomogeneities in the geomagnetic and interplanetary magnetic fields (Owens and Jokipii, 1972) (Owens and Jokipii, 1973). The present experiment is well adapted to study these statistical effects, but this short report, which is based upon a preliminary analysis of the data, will focus, instead, upon an interesting short term effect associated with a flare injection of solar protons. Specifically, a brief increase (20 min duration) in the intensity of $\sim$100 MeV protons was seen at a delay time consistent with that expected for the coherent propagation of a localized group of particles from sun to earth (Earl, 1973). This interpretation suggests that the phenomenon designated by Lin (1970) as "scatter free propagation" occurs not only at the low rigidities of kilovolt electrons but also, on occasion, at high rigidities where only diffusive propagation has heretofore been considered.

2. Instrumentation. The hodoscope is shown in Fig. 1. The detector elements are 7 trays of 27 geiger tubes with successive layers perpendicular to one another, 3 plastic scintillation counters, and a lucite Cerenkov counter. Geiger tubes in the top four trays are individually connected to coincidence circuits which, when triggered by a particle whose trajectory is suitable for detailed analysis, initiate a readout cycle that takes 23.6 msec to transmit trajectory, pulse height and housekeeping information for each event.

Sandwiched between the 2nd and 3rd trays is a 2.5 cm thick plastic scintillator to measure dE/dx for incident particles. Below the fourth tray, are two 14 cm thick plastic scintillators which record the ionization of stopping particles in two energy ranges; (90 to 170 MeV/nucleon and 170 to 230 MeV/nucleon). Each is viewed by two RCA 8055 photomultiplier tubes. Between these calorimeter counters, is a 5th tray (not shown in Fig. 1) to define those events which stop in the first counter. Two additional crossed trays below the second scintillator define the upper limit of 230 MeV/nucleon for the detection of stopping particles. Analysis, however, proceeds in two additional energy ranges defined by the presence or absence of an output from a 5 cm thick Lucite Cerenkov counter viewed by nine photomultiplier tubes. The threshold of this detector is 400 MeV/nucleon.

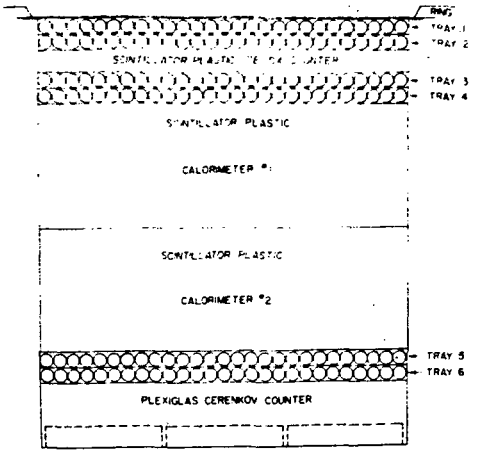

Fig. 1. The hodoscope detector.

Many details of this system are similar to those of smaller instruments flown in the past which incorporated 15 cm square detector elements with 9 tubes in each tray (Rygg and Earl, 1971; Earl, Neely and Rygg, 1972). However, the geometrical factor of 200 cm^2 sterad resulting from the present increased size of elements (50 cm) is two orders of magnitude larger than typical satellite detectors and 10 to 20 times that of balloon-borne detectors traditionally employed to detect protons and helium in the energy range of interest here. The telemetry system, operated at a 16 KHz bit rate, provides nearly error-free transmission of approximately 30 events/sec. with multiparameter pulse height analysis and trajectory information available for each event.

Representative flight data from a one hour period at ceiling are presented in Fig. 2 as contour lines plotted on a plane whose ordinate and asscissa are pulse heights in the dE/dx and calorimeter #2 counters, respectively. The numbers on these axes refer to logarithmic intervals each of which represents a factor of (4/3). Thus, 8 channels corresponds to a factor of 10. The number of events per cell associated with each curve refers to particles which stopped in calorimeter #2 with no evidence of multiplicity in any of the trays. The clear resolution of components evident in Fig. 2 is, in part, due to the discrimination against interactions made possible by the hodoscope, and, in part, due to the good resolution in ionization measurements made possible by thick scintillators and efficient light collection. The intensities presented later of 90-108 MeV protons were derived from matrices, similar to that in Fig. 2, in which were collected particles stopping in the first calorimeter.

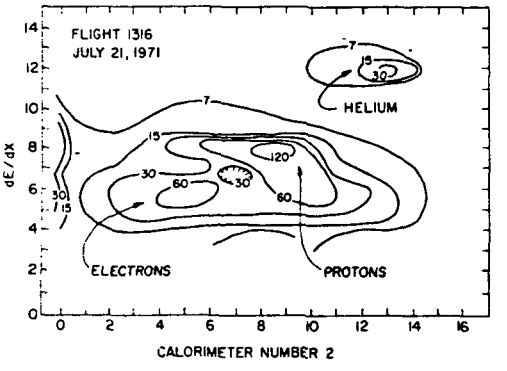

Fig. 2. Pulse height matrix for particles stopping in the second calorimeter counter.

3. The Coherent Event. The instrument has been flown on balloons launched at Churchill, Manitoba on the following four dates: July 18, 1971; July 21, 1971; July 21, 1972; July 26, 1972. All of these flights were successful. Both 1972 flights recorded solar particles from the active region that later gave rise to the great events of August 1972, but the phenomenon to be discussed here was probably not associated with that region.

The coherent event occured during Flight 1330 on July 22, 1972. Starting at about 0500UT, a slowly varying influx of solar particles began. This influx, which probably came from a flare on the back of the sun, shows velocity dispersion and is worthy of study on its own merits, but the feature of real interest appears in Fig. 3 where the flux of 90-108 MeV protons increased briefly by about a factor of 2 over the nearly constant flux of solar protons from the earlier event. Both the onset of this increase at 1150UT and the termination at 1109UT took place in less than one minute which is the interval during which counts were accumulated for the points in Fig. 3. Because these abrupt changes seemed remarkable, we looked into the interplanetary configuration at the time of the event and found the situation depicted in Fig. 4. There was a small flare at 1025UT almost exactly at the foot of the interplanetary magnetic field line which passed through earth. This flare emitted x rays detected by an ionization chamber flown as an independent experiment on the same balloon (H.R. Anderson, private communication). By coincidence, the asymptotic viewing direction from Churchill for 100 MeV protons (McCracken, 1962, Fig. 1.2) happened to be within 10° of the field direction.

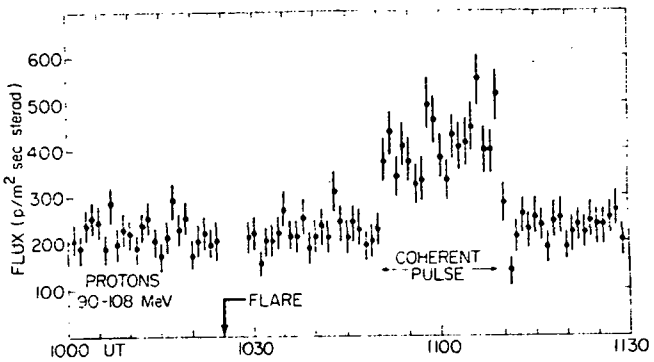

Fig. 3. Solar proton fluxes on July 22, 1972.

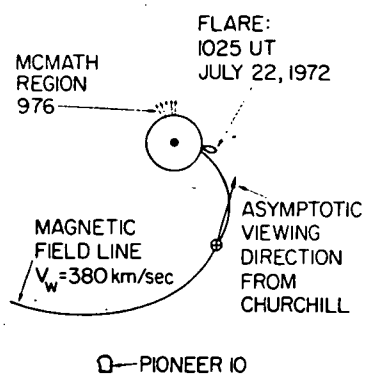

Fig. 4. The solar neighborhood during the coherent event.

The facts that the increase in Fig. 3 was most prominent in the lowest energy channel as is expected for a steep solar particle spectrum and that it occurred shortly after a well documented flare leave little reason to doubt the association between the event and the west limb flare. However, the temporal profile of the pulse is completely incompatible with diffusion models that are frequently invoked in the interpretation of solar particle injections. On the other hand, the qualitative form and quantitative details of the profile are predicted as manifestations of a novel coherent mode of propagation (Earl, 1973). In brief, particles can propagate from sun to earth along interplanetary magnetic field lines in localized groups which move with characteristic speeds comparable to the particle velocity. In particular, it is predicted that the leading edge of the coherent disturbance will move with speed 0.8V = 0.34C where V. = 0.42C is the velocity of a 100 MeV proton and C is the speed of light. This speed is in good agreement with a value

of 0.36C calculated from the 1500 sec interval between flare and pulse onset assuming a typical distance of 1.1 AU between sun and earth along the interplanetary field line. The pulse in Fig. 3 does not resemble the characteristic Gaussian profile expected for a coherent disturbance long after injection. However, the observed square profile is consistent with the shape predicted shortly after injection under conditions such that the intensity of interplanetary magnetic fluctuations is very low. The angular distribution of particles in the coherent disturbance is very anisotropic with maximum flux being expected along the field line direction coming from the sun and zero intensity being expected from the antisun direction. Fortunately, our viewing direction (See Fig. 4) was just right for observing the coherent effect but we have no way of telling whether or not the intensity was small in the opposite direction.

4. Discussion. The effect noted here is qualitatively very similar to the so called "scatter free propagation" of low energy solar flare electrons (Lin, 1970). Moreover, the theory which describes coherent propagation not only gives a convincing explanation of both these phenomena but also it relates them to conditions in interplanetary space. In particular, the spectral index $q \gtrsim 2$ of the magnetic power spectra observed by Sari and Ness (1969) is such that prominent coherent effects are expected, and the pronounced variations observed in magnetic fluctuations (Siscoe, Davis, Coleman, Smith and Jones, 1968) suggest that, on some occasions such as the present one, the spectral intensity is so low that nearly pure coherent propagation could occur. However, we have access to no magnetic data that would confirm this suggestion. In any case, the identification of a coherent effect at relatively high rigidities should stimulate further work leading to improved understanding of the acceleration of energetic particles in solar flares. In this connection, it is worth noting in Fig. 4 that the Pioneer 10 spacecraft was quite close to the same line of force on which the coherent pulse was seen at earth. Thus, it might prove fruitful to search for a similar pulse recorded there after a delay determined by particle velocities and the distance between spacecraft and earth.

Solar particle influxes which arrive at earth via the coherent mode are much more closely related to phenomena on the sun than are those which arrive after diffusion. Subject to the validity of the interpretations given above, we exploit this fact to conclude from the abrupt onset in Fig. 3 that the injection, at the sun, of 100 MeV protons occurs on a time scale of less than one minute.

Acknowledgements. This research was supported by the National Aeronautics and Space Administration under NGR 21-002-066.

References

Earl, J.A., 1973, Univ. of MD Tech. Rept. No. 73-098.
Earl, J.A., Neely, D.E., and Rygg, T.A., 1972, J. Geophys. Res., 77, 1087.
Lin, R.P., 1970, J. Geophys. Res., 75, 2583.
McCracken, K.G., 1962, J. Geophys. Res., 67, 423.
Owens, A.J., and Jokipii, J.R., 1972, J. Geophys. Res., 77, 6639.
Owens, A.J., and Jokipii, J.R., 1973, Ap. J., 181, L147.
Rygg, T.A., and Earl, J.A., 1971, J. Geophys. Res., 76, 7445.
Sari, J.W., and Ness, N.F., 1969, Solar Phys., 8, 155.
Siscoe, G.L., et al., 1968, J. Geophys. Res., 73, 61.

HODOSCOPE MEASUREMENTS OF THE SPECTRUM OF COSMIC ELECTRONS BETWEEN 10 GeV AND 100 GeV

Charles A. Meegan and James A. Earl

Department of Physics and Astronomy, University of Maryland
College Park, Maryland (USA) 20742

ABSTRACT

In an attempt to reduce divergences among independent measurements of the electron spectrum above 10 GeV, electrons were detected with the aid of a large hodoscope which incorporates 8 trays of Geiger tubes and 10 scintillation counters into a calorimeter containing 33 radiation lengths of lead. This instrument has been thoroughly calibrated up to 9 GeV at the Cornell Electron Synchrotron and has been flown twice at a depth of 5 g/cm^2 for a total of 30 hours at ceiling. Electron showers at 10 GeV are completely contained within the calorimeter where their ionization is sampled twelve times, and where hodoscope trays provide information on the geometrical distribution of shower particles. Reliable identification of electrons was ensured by extensive information on individual events together with good statistical accuracy resulting from the long exposure time and the large geometric factor (335 cm^2 sterad). Electrons appeared in a histogram of number of events vs. a χ^2 measure of goodness of fit to electron shower curves as a clearly resolved peak standing well above the nuclear background. Detailed characteristics of events in this peak are very similar to those of electron events recorded during calibrations. In particular, the initial ionization and the lateral spread of shower particles are consistent with those of calibration electrons. In contrast, the behavior of the nuclear continuum associated with minimum ionizing incident particles is different from that of calibration electrons but similar to that of nuclear events associated with incident helium nuclei. The differential electron spectrum from 10 to 100 GeV was obtained and will be presented.

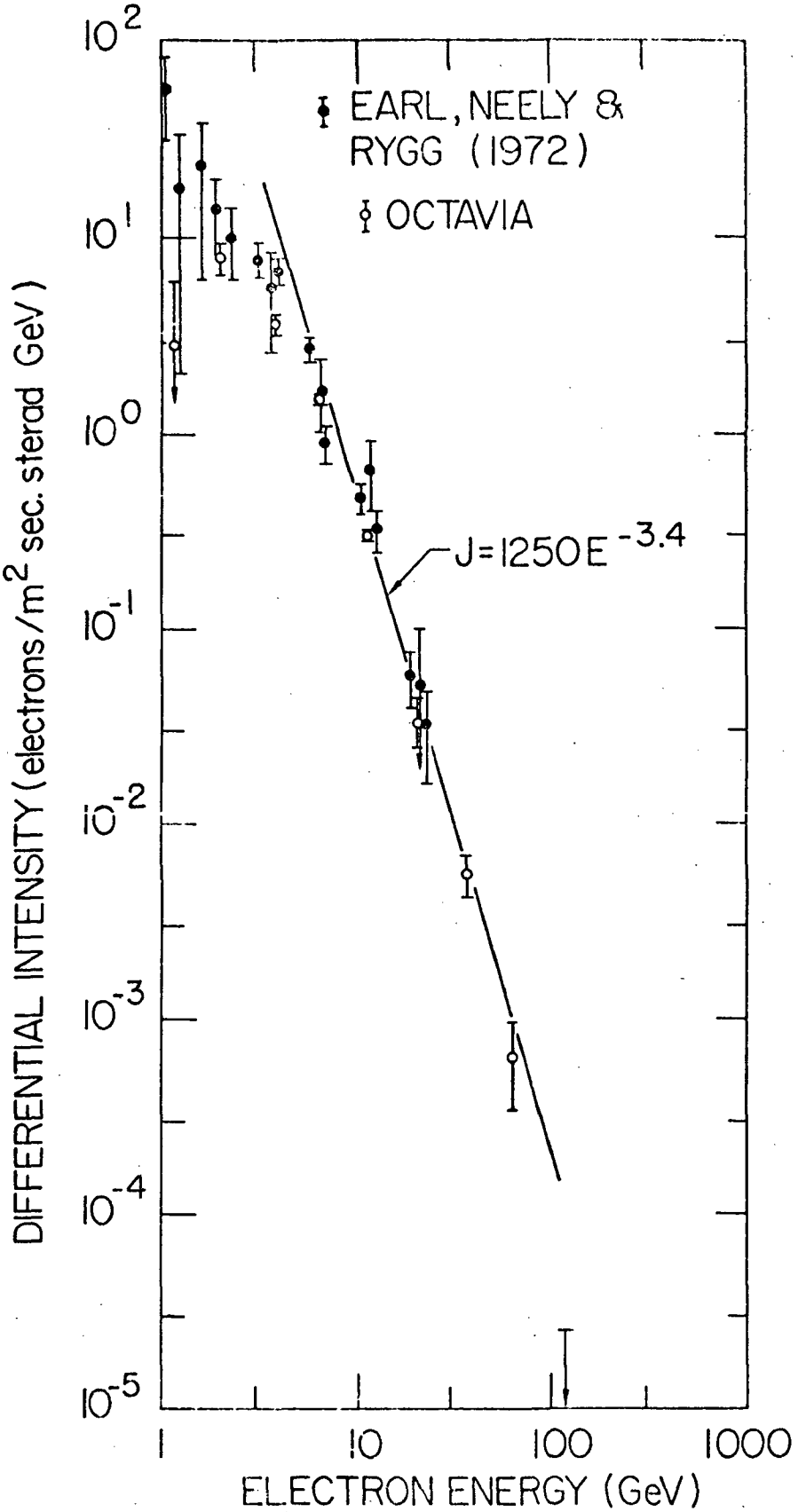
EARL, NEELY & RYGG (1972)
OCTAVIA
J=1250E^-3.4
DIFFERENTIAL INTENSITY (electrons/m^2 sec. sterad GeV)
ELECTRON ENERGY (GeV)
10^2
10^1
10^0
10^-1
10^-2
10^-3
10^-4
10^-5
1
10
100
1000

Technical Report #73-136

CHEMICAL ABUNDANCES OF COSMIC RAYS >4.5 GV MEASURED WITH A LARGE AREA PROPORTIONAL COUNTER-SCINTILLATION COUNTER STACK

Jacques L'Heureux and C.Y. Fan

Department of Physics, University of Arizona
Tucson, Arizona (USA) 85721

G. Gloeckler* and R. Mainardi

Department of Physics and Astronomy, University of Maryland
College Park, Maryland (USA) 20742

A 6500 cm^2-ster cosmic ray detector consisting of twelve gas counter trays sandwiched between two large area circular scintillation counters was flown from Palestine, Texas in November of 1972 to study the composition of primary particles >1.5 GeV/nucleon in the charge range 3 to 30. For each analyzed event, we record i) the particle trajectory using four 20 wire proportional counter trays, ii) the energy loss in each of the solid counters and iii) the dE/dx losses in each of the twelve gas counters. The large dynamic range of the detector is established by operating six of the gas counters in the ionization mode. A description of the instrument and some preliminary results are given.

1. Introduction. Present cosmic ray propagation models (see e.g. Shapiro and Silberberg, 1970) suggest that the measured abundances of C,O, and Fe at the earth are closely related to their compositions at the sources, whereas the amount of lighter elements (Li,Be, and B), which are the fragmentation products of the heavier ones, reflects how much material was traversed by the primaries before they reach the earth. The composition versus energy for particles below 10 GeV/nucleon has been quite well studied and the results show a similar spectral shape for all elements. For particles of energies above 10 GeV/nucleon, however, the picture is quite different.

Many groups have in the past year reported steepening differential energy spectra for secondary as compared to nuclei of mostly primary origin like C,O, and Fe (Balasubrahmanyan and Ormes, 1972; Juliusson et al., 1972; Webber et al., 1972; Smith et al., 1973). Some of these groups have in addition reported a slightly flatter Fe spectrum when compared to C and O (Balasubrahmanyan and Ormes, 1972; Webber et al., 1972; Juliusson and Meyer, 1973). It is therefore clear that important information regarding particle sources as well as particle propagation in the interstellar medium can be obtained from high energy composition measurements.

The instrument which we have designed to study this problem has the following desirable characteristics: 1) a large geometrical factor to detect a sufficient number of relativistic heavy cosmic rays and ii) a low mass

---

* Alfred P. Sloan Foundation Fellow.

to minimize the fragmentation probability of the incident particles in the instrument and to reduce the unwanted background induced by particles which may enter from the side. The light weight is also necessary to permit the instrument to reach high balloon altitudes.

The instrument was constructed and flown on a high altitude balloon on November 4, 1972. The analysis of the data is in progress. This paper reports the preliminary results.

2. Instrumentation.

A schematic diagram of the instrument is shown in fig. 1. The main telescope consists of two circular plastic scintillation counters (NE-102) labelled as S1 and S2. Each one is set in a light diffusion box and is viewed by four photomultiplier tubes. Each scintillator is used for a dE/dx measurement of the incoming particles. The geometry factor is 6480 cm^2-ster. Sandwiched between these counters, there is a stack of gas proportional/ionization counters. The gas counters are in the form of 12 trays, each tray being subdivided into 20 separate counters. The square trays are 102 cm on the side and 5.1 cm thick. The 20 individual chambers are identical in dimension, 5.1 by 5.1 by 102 cm, each of which has a single high voltage wire at the center. The ground planes between trays and the partitions between the counters are made of wires spaced 1.27 cm from each other. All of the trays fit inside a common gas enclosure filled with a mixture of 90% argon and 10% methane at a pressure of one atmosphere. The gas pressure is maintained to an accuracy of 0.25%.

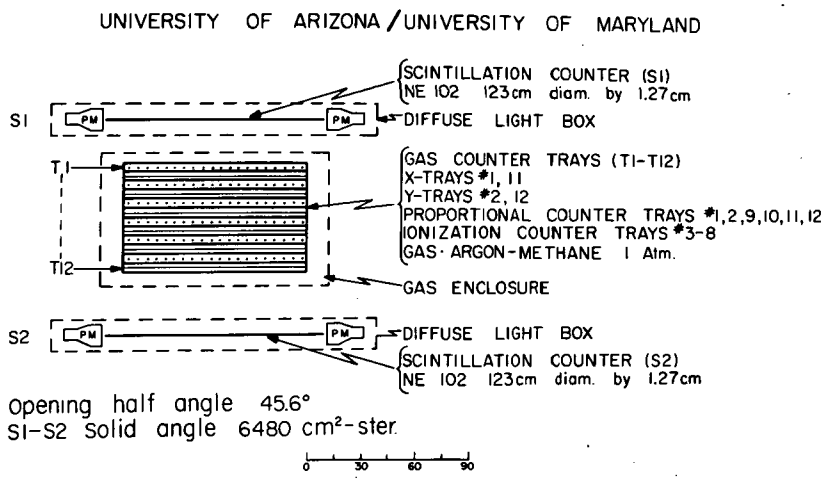

Fig. 1. Schematic cross section of the instrument.

The twelve trays, although identical in construction, are assembled with their center and partition wires alternatively in the X and Y directions. They are also operated in one of two modes. The top two and the bottom four are operated at 1550 volts in the proportional mode while the remaining six are in the ionization mode at 550 volts. The ionization trays are used for the dE/dx measurement of VH and VVH cosmic ray nuclei (Z>20) since they are not expected to saturate at high ionization levels. Four of the six proportional trays (the top and the bottom two) are used to locate the X-Y position of the particle trajectory. This position information is used to compensate for path length differences, to correct for any non-uniformities in the scintillation and in the gas counters. The outputs from each individual wire chamber are summed for each tray and each of the 12 resultant pulses is digitized with a 10 bit A-D converter.

For each particle which penetrates through the detector system, we perform two dE/dx measurements in the plastic scintillation counters and six dE/dx measurements in the gas counters. For particles of charge less than 15, the six proportional counters are used while for nuclei of higher charge, an additional six measurements are made in the ionization chambers. Since the dE/dx in a solid scintillator is relatively constant over the entire relativistic range, the two dE/dx measurements are sufficient for the charge determination of the particle. For the energy determination, we attempt to use the known fact that the ionization loss in a gas counter by a relativistic particle increases logarithmically with energy in the range from 2 to 200 GeV/nucleon (Crispin and Fowler, 1970) to measure their spectra in this limited range.

The first flight with this instrument took place on November 4, 1972 from Palestine, Texas. The experiment was aloft for a period of 7.5 hours, 5.7 of which were at an altitude of about 129,000 ft (3.2 g/cm^2). The vertical cutoff rigidity at the gondola position varied from 4.5 to 3.1 GV.

3. Data analysis and results. During the 5.7 hours at the floating altitude, 120,000 events of charge greater than 3 were analyzed, 32,000 of which had a clean trajectory and were used for the determination of the composition spectrum. The non-uniformities in the scintillator response vs. position were studied, using in-flight Carbon and Oxygen nuclei. The response function thus obtained was used in subsequent corrections to the energy loss measurements. A charge spectrum, obtained using only the scintillator outputs corrected for the non-uniformities and for the path length differences, is shown in Fig. 2. In this plot, Carbon has a full width at half maximum (FWHM) of 7.6% corresponding to ±0.2 charge units. The resolution, as expected, varies as 1/Z as we go to nuclei having a higher charge. The saturation effect in scintillation counters however degrades the resolution reducing it to ±0.5 charge units at Fe. Our preliminary charge composition is in agreement with earlier work.

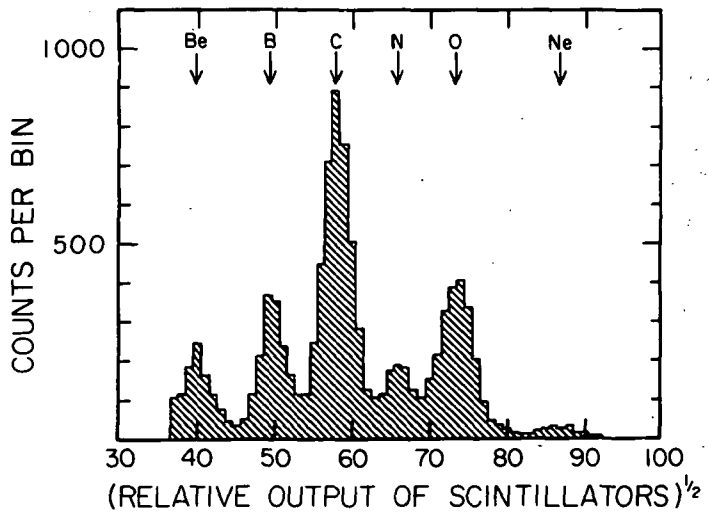

Fig. 2. Charge spectrum from the scintillators corrected for their non-uniform response.

The saturation effect in NE-102 scintillation material is shown in Fig. 3, where we have plotted the ratio of the light output to the energy loss (dL/dE), as a function of energy loss. The energy loss scale is relative to that produced by a singly charged relativistic particle. Notice that the light reduction at Fe is 0.42, crowding the elements by a factor of 2.5 in this charge region.

The analysis of the wire chambers for the energy measurement is yet to be completed. To illustrate the feasibility, a scatter plot of the scintillator dE/dx vs. the gas counter dE/dx is shown in Fig. 4. The gas counter dE/dx is the average of two wire trays which seemed to give the best performance during the flight. Clusters corresponding to the elements from Be to Ne are marked. The solid curves in the plot indicate the expected responses vs. energy when the logarithmic relativistic rise in the energy loss in the gas chamber is included. We hope that the results will show a marked improvement when all six gas trays are used.

4. Acknowledgements. We gratefully acknowledge the valuable contribution to this program from Messrs. Cain, Tums and Isaksen at the University of Maryland and from Messrs. Hudor, Mioduski, Oona, and Rothchild at the University of Arizona. We are also indebted to the staff of the National Center for Atmospheric Research Balloon Facility for their excellent support of the flight.

This work was supported in part by NASA under grants NGR 03-002-107 (University of Arizona) and NGR 21-002-224 (University of Maryland). Travel to the launch site for the Arizona members of the team was supported by the NSF Institutional Research Grant from the University of Arizona. We are also grateful to the State of Arizona for providing free computer services on the University computer.

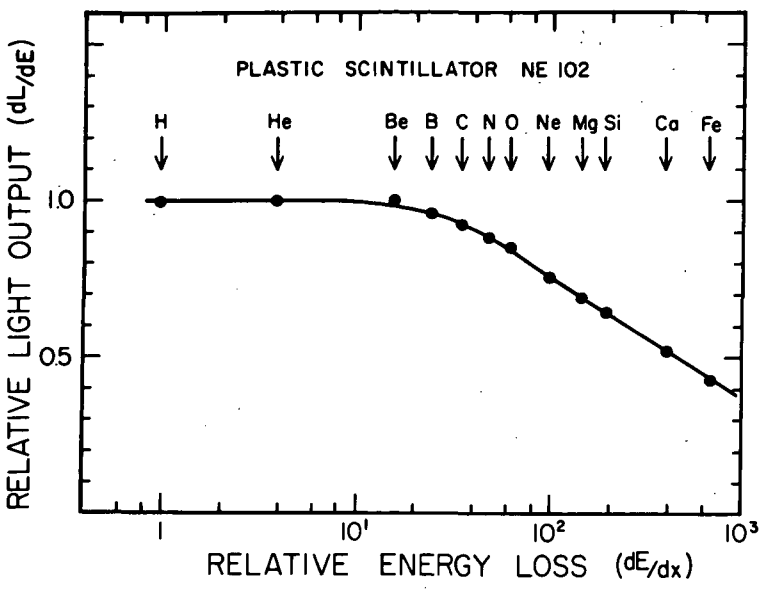

Fig. 3. Saturation effect in NE-102 scintillator material for relativistic heavy nuclei. Plotted is the ratio of the light output to the energy loss (dL/dE). The energy loss scale is relative to a singly charged relativistic particle.

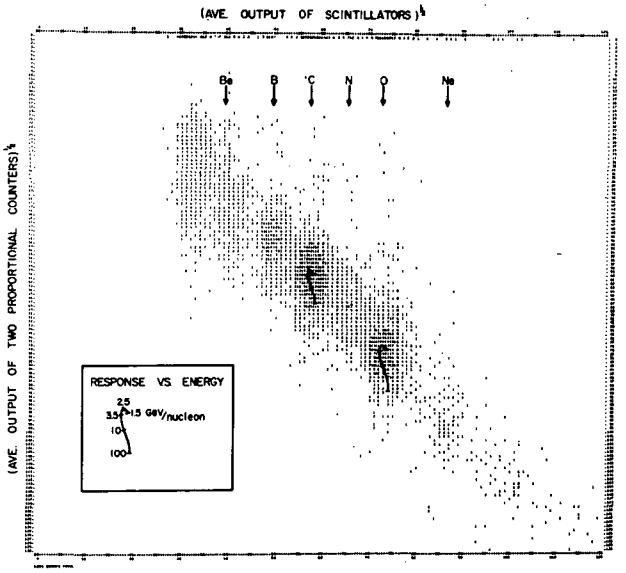

Fig. 4. Scatter plot of the scintillator energy loss versus the gas counter energy loss. The solid curves represent the expected response versus energy for Carbon and Oxygen. Note that the square root of the energy loss is used to linearize the scales.

5
415

5. References.

Balasubrahmanyan, V.K., and Ormes, J.F., Goddard Space Flight Center preprint X-661-72-447, Dec. 1972.

Crispin, A., and Fowler, G.N., Rev. Mod. Phys. 42, 290, 1970.

Juliusson, E., Meyer, P., and Muller, D., Phys. Rev. Letters, 29, 445, 1972.

Juliusson, E., and Meyer, P., Bull. of the Am. Phy. Soc., 18, 540, 1973.

Shapiro, M.M., and Silberberg, R., Ann. Rev. Nuc. Sci., 30, 323, 1970.

Smith, L.H., Buffington, A., Smoot, G.F., Alvarez, L.W., Wahlig, W.H., Ap. J. 180, 987, 1973.

Webber, W.R., Lezniak, J.A., Kish, J.C., and Damle, S.V., preprint, Oct. 1972.

Technical Report #73-137

INTENSITY OSCILLATION OF LOW ENERGY SOLAR PARTICLES OBSERVED ON THE IMP 7 SATELLITE

C. Y. Fan,[1] G. Gloeckler[2] and D. Hovestadt[3]

[1]Department of Physics, University of Arizona
Tucson, Arizona 85721, USA

[2]Department of Physics and Astronomy, University of Maryland
College Park, Maryland 20742, USA

[3]Max Planck Institut für Extraterrestrische physik
8046 Garching, Germany

Solar flare particles in the energy range from 125 to 160 KeV per charge were detected and analyzed by an electrostatic deflection vs. energy instrument on board the Explorer 47 (IMP 7) satellite. A harmonic analysis of the counting rates shows that frequently, the fluctuation of the particle flux can be approximately represented by $N(t) = f(t)\sin 2\pi\nu t$ where $f(t)$ is a smoothly varying function of t. The oscillation frequency ν varies from flare to flare and is of the order of 2×10^{-3} ~/sec. The physical implications of the finding will be discussed.

1. Introduction. The propagation of solar flare particles has been studied both theoretically and experimentally for many years. It is now generally agreed that, after the impulsive injection of the particles from the sun, the motion of the particles in the interplanetary space can be described as the superposition of a diffusion in a static magnetic field and a convection with the field lines carried outwards by the solar wind. The diffusion tensor K can then be related to the power spectrum of the interplanetary magnetic field, (see e.g. J. R. Jokipii, 1971). In these studies, however, no attempt was made to investigate transient phenomena such as intensity variation due to solar wind fluctuations, shock waves, and hydromagnetic waves, although these phenomena may contain important information relating to the mechanism of releasing particles from the active regions of the sun, or the modulation of particle intensity by magnetohydrodynamical waves. The purpose of this paper is to report a new phenomenon of the intensity variation of solar flare particles observed with a detector system on the IMP 7 satellite. It was found that frequently the intensity showed sinusoidal fluctuations of frequencies $\sim 2 \times 10^{-3}$ ~/sec, and the durations of the fluctuations were about one hour. The physical implication of the finding is discussed.

2. The Detector System and the Satellite. The detector system used for the experiment is an electrostatic deflection vs. energy instrument. A schematic drawing of the instrument is shown in Fig. 1. It was designed to detect ions, electrons and positrons with energies as low as 100 KeV/charge. Particles which enter the collimator are deflected in one of the three electrostatic field regions and strike one of the ten detectors. The amount of deflection d of a particle in the field regions is related to the energy T and the charge Q of the particle by the following expression: $d = gQV/T$, where V is the voltage difference between two deflection plates

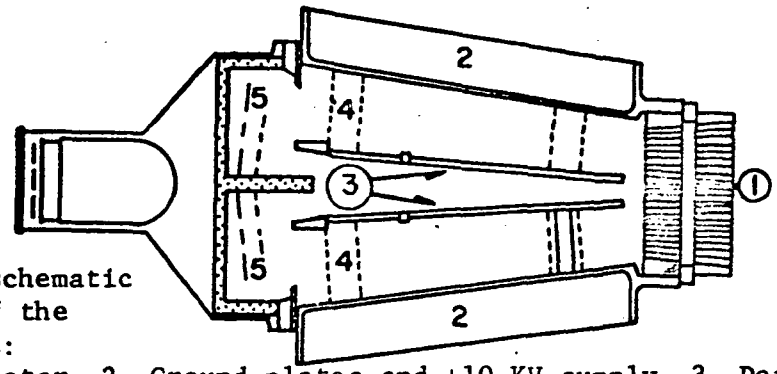

Fig. 1. A schematic diagram of the instrument:
1. Collimator, 2. Ground plates and ±10 KV supply, 3. Deflection plates, 4. Standoff insulator, 5. 10 Solid state detectors.

of the given field region, and g is the characteristic constant. Therefore, in this instrument, the range of the energy per charge of an ion, $\Delta(T/Q)$, is determined by the position and the size of the detector triggered. T and Q can thus be determined separately by an additional measurement of the energy deposit of the ion in the detector. The details of the system have been published elsewhere (Fan, Gloeckler and Tums, 1971).

The voltages applied to the deflection plates are -10 KV, +10 KV. At these voltages, the ranges of the energy per charge of positive ions and electrons for the ten detector channels are from 0.125 to 1.90 MeV/Q. However, for the solar flare events reported in this paper, only the 0.125-0.160 MeV/Q energy channel, P1, recorded rates high enough for the study.

The apparatus was launched into space on September 22, 1972, on the IMP 7 satellite whose orbit has an apogee 38 earth radii and a perigee 34 earth radii. Because of its large near circular orbit, solar flare particles can be measured even when the satellite is in the tail region of the earth's magnetosphere.

3. The Data, Method of Analysis and Results. The counts of the P1 are accumulated over four readout periods, i.e., 4 x 1.27843 sec, for the transmission by the satellite data system to the ground. These counts, after the subtraction of quiet time counting levels, yield the intensity profiles of solar events in these channels. Fig. 2 shows the P1 rate for a portion of the event observed on day 287 (October 13), and Fig. 3 gives the P1 rate observed on day 292 (October 17). The positions of the satellite in these time intervals are indicated by the sun-earth-probe angles, designated as $\angle$ SEP in the Figures. The rates in higher energy channels are much lower and are not presented here. The rates in the electron channels are practically the same as the background level. From the pulse height information, it was found that more than 95% of the particles recorded are protons.

One distinguishing feature of the intensity-time profiles of these events is that they appear to be very rugged, having an appearance of saw teeth. The amplitudes of the fluctuations are far larger than statistical. In order to understand the nature of these features, an autocorrection function is constructed for the counting rates in each of the peaks shown in Fig. 2 and Fig. 3. Let $N(k\tau)$ = counting rate recorded at

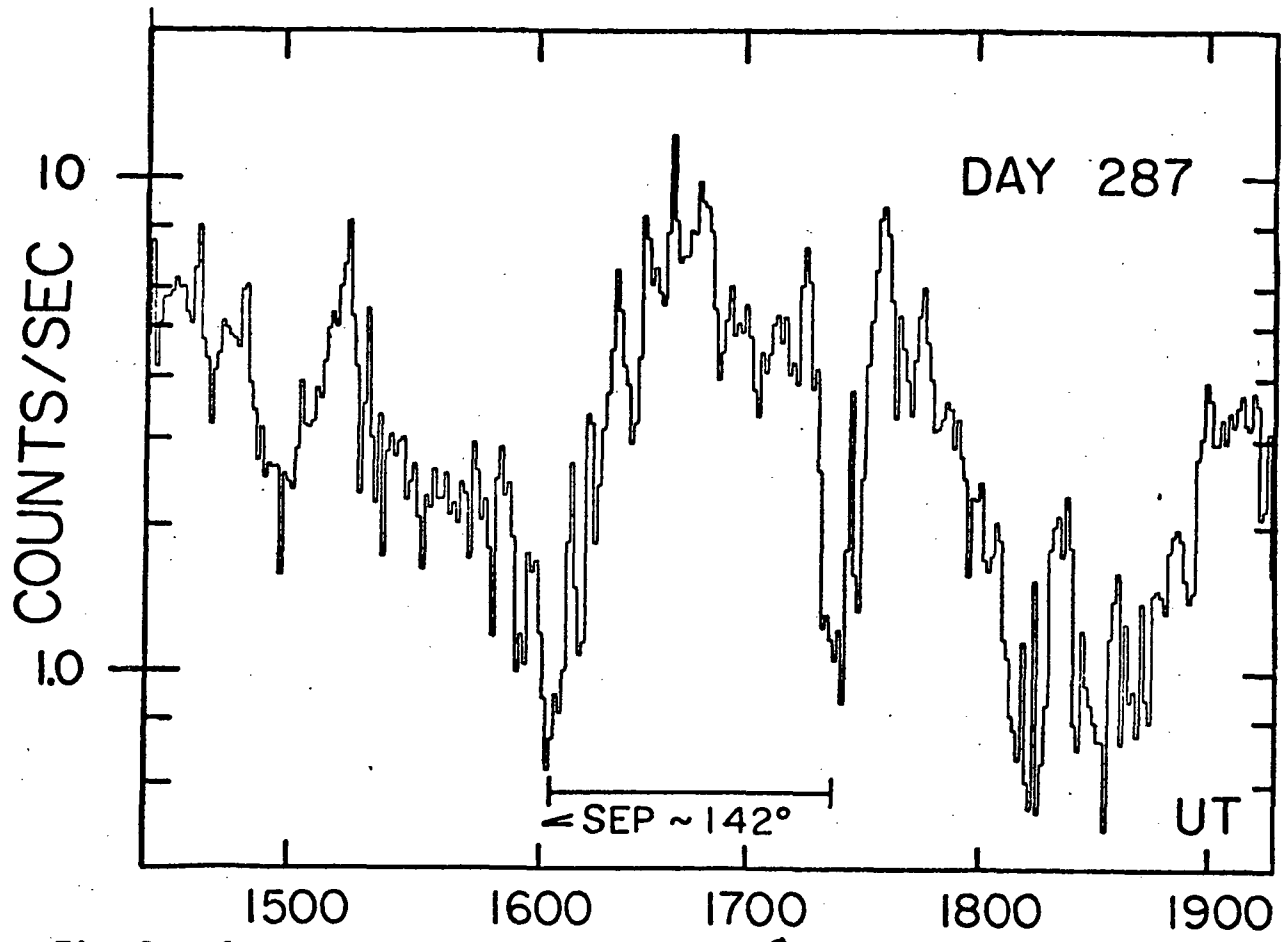

Fig. 2. P1 counting rate, day 287, 1972.

Fig. 3. P1 counting rate, day 292, 1972.

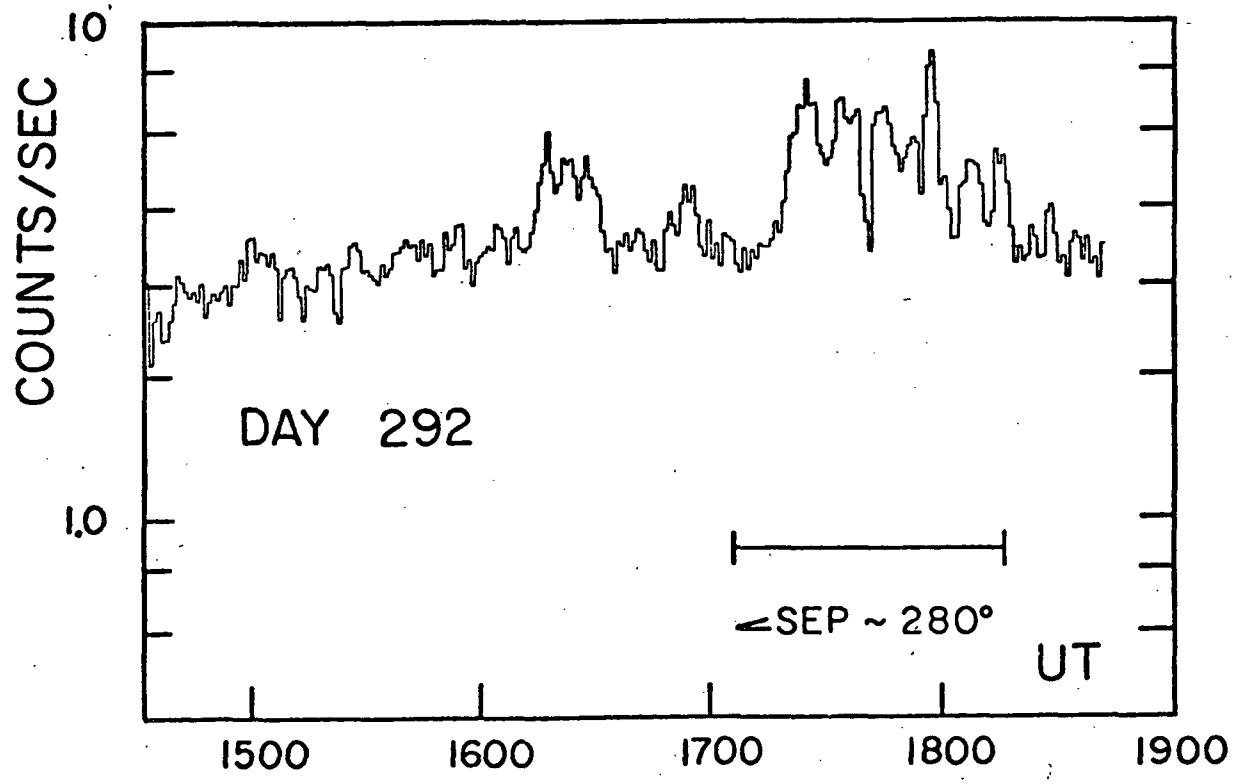

$t = k\tau$, where k is a positive integer and τ is the time interval between two neighboring data points. The quantity τ is usually an integer m times the basic readout period $\tau_r = 1.27843$ sec. If K = total number of data points, the correlation function C is defined by the following expression:

$$C(\Delta k) = \frac{1}{K-\Delta k} \sum_{k=0}^{K-\Delta k-1} N(k\tau)N((k+\Delta k)\tau).$$

Two selected samples of the function are displayed in Fig. 4. These results

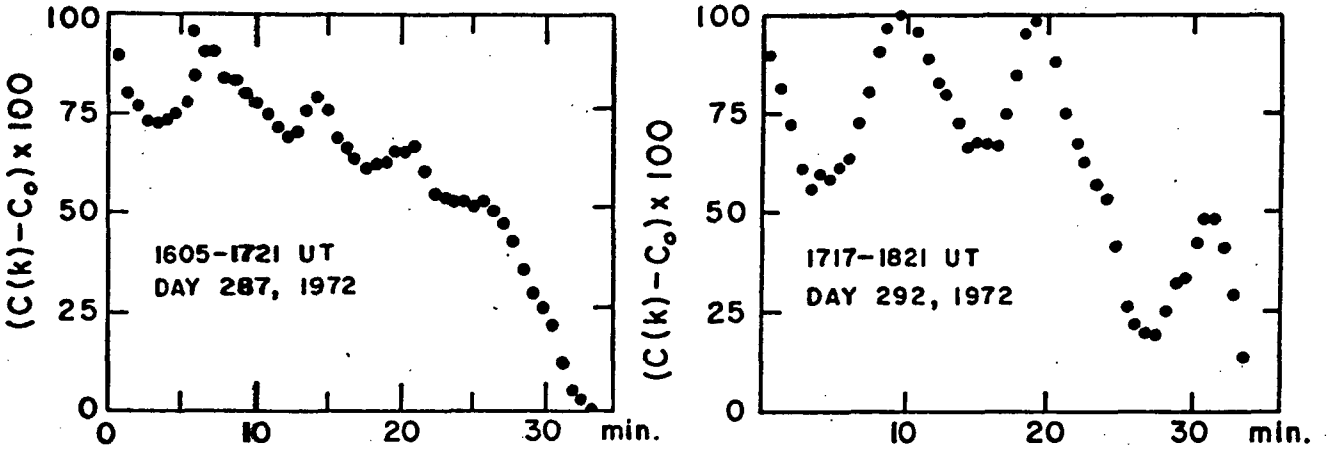

Fig. 4. Correlation functions of the counting rates plotted in Fig. 2 and Fig. 3, respectively.

indicate that in these two time intervals, the P1 counting rates can be represented by $N(t) = f(t)\sin 2\pi\nu t$ where f(t) is a smoothly varying function of t, and ν's for these two events are respectively 2.45×10^{-3} and 1.66×10^{-3} ~/sec. We have examined six other similar cases which were observed in the period from September 30 to November 6, 1972 (Days 274-311) for which the data tapes were available to us. The frequencies of the oscillation varied from 1.5×10^{-3} - 3.0×10^{-3} ~/sec. The physical implications of the oscillation will be discussed in the next section.

4. Discussion. The intensity oscillations which we have observed cannot be due to the release mechanism of the particles at the sun. This conclusion is based on the fact that the energy window of the P1 channel is ~35 keV, and thus the dispersion in the arrival time for the particles in this energy band from the sun to the earth's orbit will completely smear out any possible oscillations whose periods are only of 5-10 minutes. We have also examined the nature of modulation of an anisotropic flux of particles by the spin of the spacecraft. We averaged the counting rate over m spacecraft revolutions, and were able to show that the oscillation amplitude of the correlation function due to the spin modulation for a flux of a degree of anisotropy "A" is $\sim A^2/(m\pi)^2$ with a frequency ν_b equal to the beat of the readout frequency (= 1/1.27843) and spin frequency of the spacecraft (1/1.3066). Because the beat frequency ν_b is 1.6×10^{-2}~/sec, about five times higher than the observed ones, and the observed amplitude is

independent of m and is one order of magnitude greater than $A^2/(m\pi)^2$ for m = 16 and A = 1, we discarded this explanation. Therefore, it is more likely that the observed oscillation is due to the modulation of the solar flare particles by the magnetic fields in the vicinity of the spacecraft.

Large amplitude fluctuation in the magnetic fields in the earth's magnetosheath was first reported by Siscoe et al. (1967). It was suggested that magnetic oscillations in the transition region are excited throughout the hydromagnetic frequency regime by the interaction between the solar wind and the magnetosphere. At the time of the measurement, the frequencies near 5×10^{-3} ~/sec showed the greatest activity. From the fact that (1) all the particle intensity oscillations reported in this paper were detected during the time when the spacecraft was in the tail region of the magnetosphere or near the bow shock and (2) the frequencies were nearly equal to 5×10^{-3} ~/sec, we conclude that the hydromagnetic waves and the particle intensity oscillations are two closely related phenomena (Jokipii, 1973).

The actual relation between the two phenomena is unknown at present. However, we can suggest the following two possibilities:

(a) The energy spectrum of the particles was modulated by the waves. If the spectrum was as steep as what was observed on day 287, (shown in Fig. 5), a small degree of acceleration or deceleration in the particle energies by the hydromagnetic waves would manifest itself as a large amplitude oscillation in the particle flux recorded by the detectors.

(b) The particles were confined to move along bundles of magnetic lines of force but there was a non-uniformity in the particle density. An intensity oscillation would then be a natural result of a "flapping" motion of the lines of force due to the hydromagnetic waves.

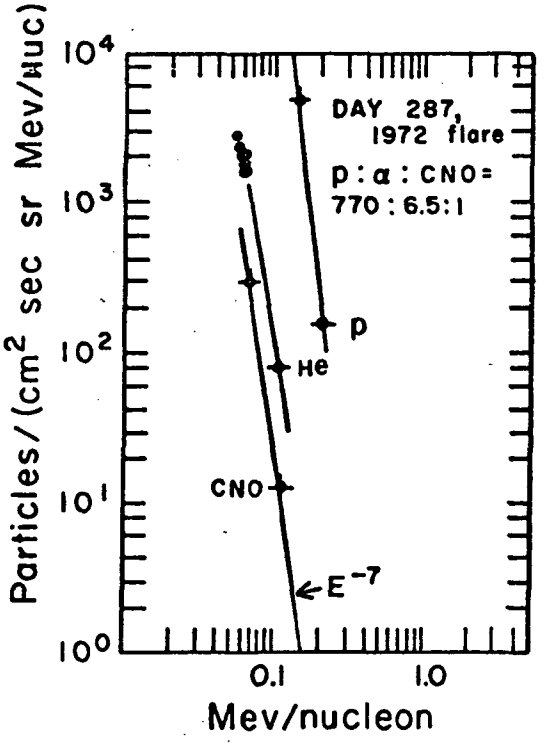

Fig. 5. Energy spectrum of solar flare proton, He, and CNO observed on Day 287, 1972.

5. Acknowledgments. This work is supported in part by NASA under grants NGR 03-002-107 (University of Arizona) and NGR 21-002-224 and NASA Contract NAS5-11063 (University of Maryland). The authors wish to express their appreciation to E. Tums, J. Cain, J. Gigante, J. Dalton, and R. Sciambi of the University of Maryland and Y. C. Lin of the University of Arizona for their contributions to this program.

References

Fan, C. Y., G. Gloeckler and E. Tums. "An Electrostatic Deflection vs. Energy Instrument for Measuring Interplanetary Particles in the Range 0.1 to ~3 MeV/charge." The 12th International Conference on Cosmic Rays, Vol. 5, 1602, 1971.

Siscoe, G. L., L. Davis, Jr., E. J. Smith, P. J. Coleman, Jr., and D. E. Jones. "Magnetic Fluctuations in the Magneto Sheath: Mariner 4." J. Geophys. Res. 72, 1, (1967).

Jokipii, J. R. "Propagation of Cosmic Rays in the Solar Wind." Reviews of Geophys. and Space Science, 9, 27, (1971).

Jokipii, J. R. This possible connection was pointed out to us by Professor Jokipii.

Technical Report #73-138

MEASUREMENT OF ELEMENTAL ABUNDANCE OF VERY LOW ENERGY SOLAR COSMIC RAYS

D. Hovestadt, O. Vollmer, G. Gloeckler[+] and C.Y. Fan[o]

Max-Planck-Institut für extraterrestrische Physik
8046 Garching, W-Germany

Heavy interplanetary particles ($3 < Z < 30$) have been observed during a solar flare period between October 29 and November 4, 1972. The nuclear abundance has been determined by a two parameter analysis (dE/dx vs E technique) of a thin window proportional counter - solid state detector device aboard the Explorer 47 (IMP-7) satellite. Energy spectra are given for C, O and Fe. The elemental abundance relative to oxygen is determined for carbon, neon, magnesium, silicon and the iron group in the energy range 0.62 to 6.9 MeV/nucleon. For the Fe/O ratio no energy dependence could be observed within the error limits.

1. Introduction. For several particle flares attempts have been made in the past to determine energy spectra and relative abundances of solar cosmic rays. Emulsion techniques at high energies (above 20 MeV/nucleon) (Bertsch et al., 1973a and references therein), active satellite experiments at energies down to about 8 MeV/nucleon (Mogro-Compero et al., 1972a, Teegarden et al., 1973), and etching techniques at energies down to 100 keV/nucleon (Price et al., 1971, Crawford et al., 1972, Fleischer et al., 1973) revealed a rough agreement of the cosmic ray abundances with the solar abundances. A considerable overabundance of iron in solar cosmic rays has been observed at low energies. Crawford et al., 1972 and Braddy et al., 1973 report an energy dependent increase of the Fe/Si and Fe/O ratio in the energy region 0.30 to 20 MeV/nucleon. Measurements of Mogro-Compero et al., 1972b indicate a high variability in the Fe/O ratio from flare to flare above 5 MeV/nucleon.

The present paper for the first time reports abundance measurements obtained with an active satellite experiment which coversthe low energy range down to about 90 keV/nucleon (for iron) The results presented in this paper go down in energy only

+ University of Maryland, College Park, Maryland
o University of Arizona, Tucson, Arizona

to about 600 keV/nucleon. Results on lower energies will be reported later, since the use of the dE/dx data of Northcliff et al., 1970 below this energy becomes increasingly questionable and a detailled analysis of calibration measurements will be necessary.

2. Instrumentation and satellite. The experiment is a dE/dx residual energy telescope using the proportional counter as a dE/dx device and the surface barrier detector for determination of the residual energy. A plastic scintillator cup serves to reject penetrating particles. The lowest energy limits for each nuclear species is determined by the total thickness of material in front of the solid state detector, which amounts to about 0.328 ug/cm^2 polyethylene equivalent, and by the electronic thresholds. The effective geometrical factor is 1.03 cm^2 ster. The isobutane gas density of the proportional counter was stabilized to within less than 0.5% over the two months of operation after launch of IMP-7. For more details see Hovestadt et al., 1971.

From calibration measurements and response calculations it turns out that at low energies, where the heavy particles are not fully stripped any more, the response tracks in a two dimensional dE/dx - E matrix merge or cross each other for different nuclear charges. Nevertheless at entrance energies above about 400 keV/nucleon a clear separation of individual even Z nuclei is possible up to iron. For higher energies the charge resolution is mainly determined by path length variation due to the finite opening angle of 21 degrees half-angle.

The satellite was launched on September 21, 1972 into a nearly circular orbit at a radial distance of about 38 earth radii. Because of the orientation of the instrument in the spacecraft and the satellite attitude the telescope scanned all directions within the ecliptic.

3. Observational result. The data were obtained during a weak solar particle flare in the period October 29 to November 4, 1972. A total of 24470 events have been accumulated over the entire period of increased heavy particle flux as indicated on figure 1 by a bar. The flux increase was very likely associated with an optical flare region near the central meridian of the sun which occurred on October 29, 1972 at about 16:00 UT. The first increase of heavy particle flux was observed about 9 hours after the optical flare. Figure 2 shows the two dimensional pulse height distribution with D1 representing the pulse height in the proportional counter and D2 in the silicon detector. Tracks for carbon, oxygen, neon, silicon, magnesium and the iron group are clearly separated.

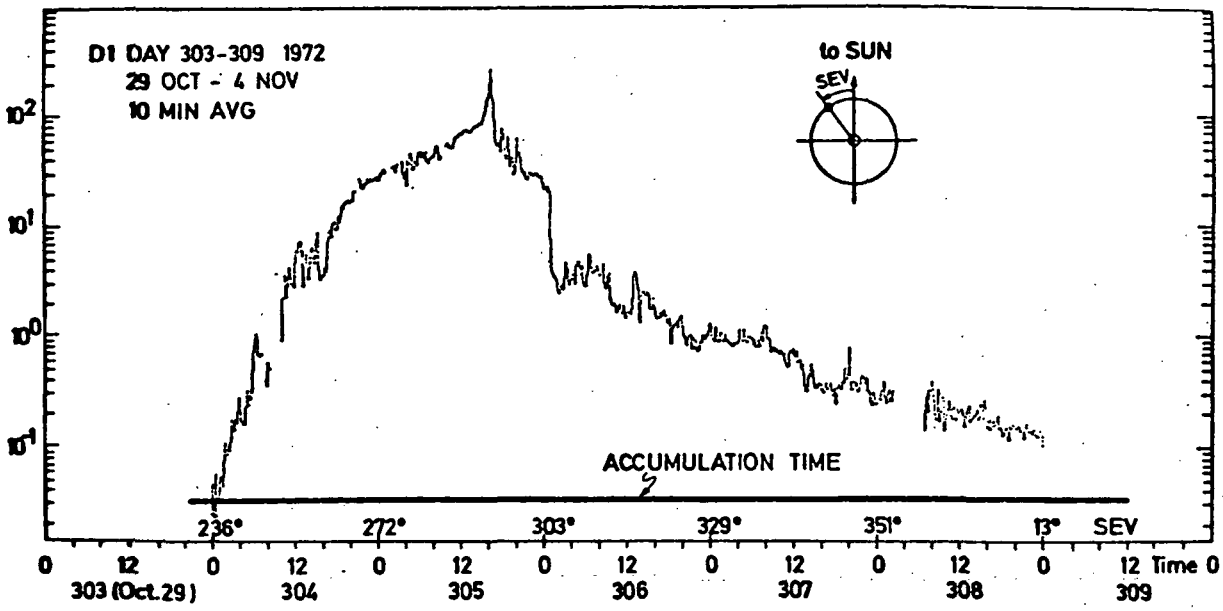

Fig. 1. Heavy ion counting rate (D1-single rate) versus time (response: carbon 0.15 - 4.6 MeV/nucleon; O: 0.12-9 MeV/nucleon; Fe: > 0.09 MeV/nucl.). The position of the satellite with respect to the sun-earth line is indicated by SEV.

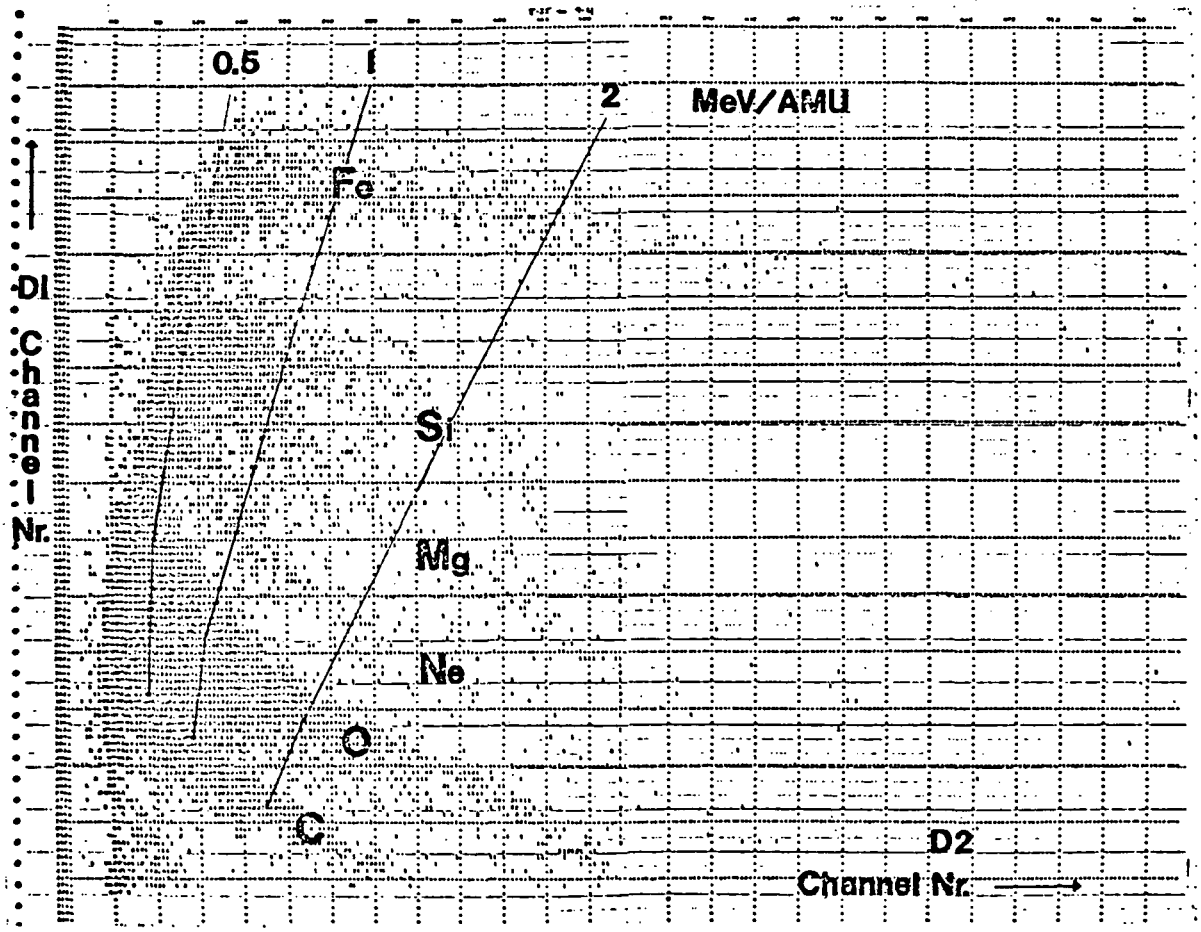

Fig. 2. Two dimensional dE/dx versus E pulse height distribution of the flare October 29 to November 4, 1972. Total number of event = 24417. D1 = proportional counter, D2 = silicon detector.

The number of particles along each track has been converted into ENERGY SPECTRA by using a calibration curve of incident energy versus D2 pulse height, based on Northcliff's et al., 1970 dE/dx-tables for heavy ions, and taking into account pulse height defects of the silicon detector as determined experimentally at a heavy ion accelerator.

Figure 3 shows the differential energy spectra for carbon, oxygen and iron. Along with the spectra is drawn a curve with the form E^{-3}, which corresponds to the spectral form of all three spectra.

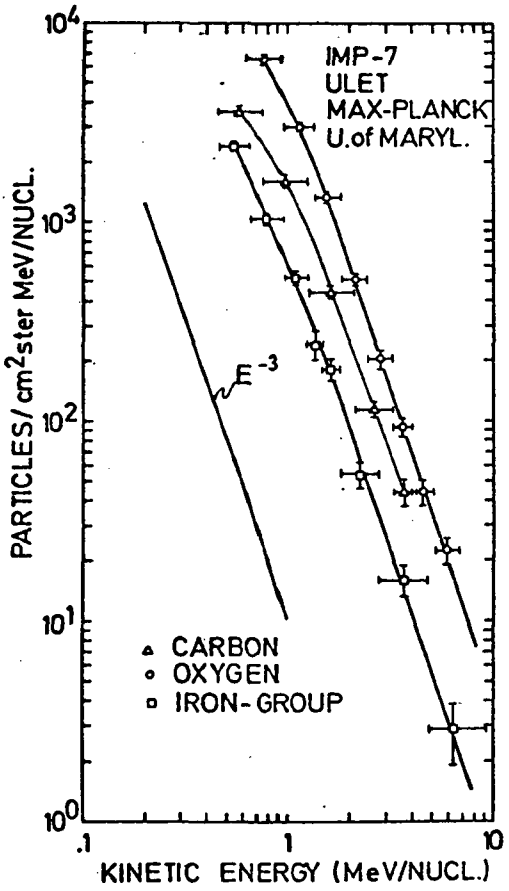

Fig. 3. Energy spectra of carbon, oxygen and the iron group derived from figure 2. To get the fluence of the flare multiply by 60.

Within a wide energy band as indicated in table 1 for each species the ABUNDANCE relative to oxygen is determined. Because of the contribution of nitrogen to the oxygen track, which is in the order of 10%, the abundance ratios are corrected by 10% compared to the pure number ratios. The result is shown in table 1 along with experimental results of other authors. The experimental errors are based on the statistical errors and enlarged by an estimated upper limit of systematic error due to uncertainties in the energy calibration.

The ENERGY DEPENDENCE of the abundance ratios for carbon and iron have been determined. Figure 4 shows the result along with similar ratios obtained by other experimenters.

Our data show a carbon/oxygen ratio of about 0.4, which is nearly independent of energy and which agrees reasonably well with the value of other authors at higher energies. The results on iron show an enhanced flux compared to the results at higher energies of Teegarden et al., and Bertsch et al.. We do not see any significant change in the ratio over the energy range from 0.62 to 6.9 MeV/nucleon, which seems to be in contradiction to Braddy et al., 1973, which is the only other data overlapping in energy with ours.

Table 1 Relative Abundance ratios (Oxygen = 1.0)

Element	Energy MeV/Nucl.	Present Work	Crawford et al.1972	Teegarden et al.1973	Bertsch et al.1972	Mogro-Compero et al.1972
C	0.62-4.21	0.43±0.02		0.49±0.03(2)	0.56±0.06	-
O	0.62-6.9	1.00	1.0	1.0	1.0	1.0
Ne	0.73-6.9	0.13±0.02	$0.1^{+.1}_{-.05}$	.127±.011(2)	.16±.03	.21±.08
Mg	0.96-6.9	0.22±0.02	.125±.03	.182±.014(2)	.056±.014	.13±.06
Si	0.89-6.9	0.23±0.03	.1	.107±.011(2)	.028±.01	.36±.12
Fe	0.62-5.2	0.17±0.02	.09±.03	.028±.005(2)	.06±.015(3)	.37±.12

(1) Original data was normalized to Si = 1.(O/Si = 10.0). (2) Sept. 1,1971. (3) Bertsch et al.1973.

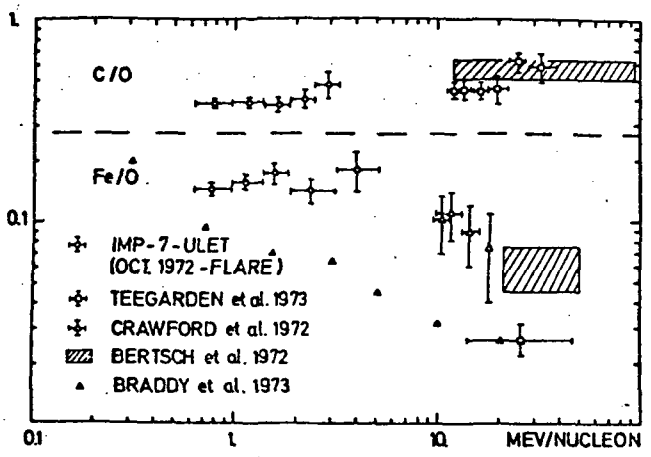

Fig. 4. C/O and Fe/O abundance ratio as a function of energy. The source of the data are indicated in the figure.

4. Discussion. From table 1 we see a reasonable good agreement of the C/O, Ne/O and Mg/O ratios with the values of Teegarden et al., 1973. The data of Bertsch et al., 1972 as measured at considerably higher energies E> 20 MeV/nucleon are a factor of five for Mg/O and a factor of eight for Si/O lower than our values.

The values of Crawford for Mg, Si and Fe are about a factor of two lower than ours. This difference may in part be explained because their data originally was normalized to silicon and had to be converted to the value relative to oxygen, which introduces additional uncertainties in the absolute values. On the other hand their data overlap in energy only at the lowest energy point (3 MeV/nucleon). Very recently Braddy et al., 1973 published data of the Fe/O ratio which completely overlap our energy range. Their Fe/O ratio is about a factor 2 lower than ours and shows a fairly strong energy dependence in a region, where we see no such differences in the abundance ratios. It should be emphasized that their and our measurements are not affected by the magnetosphere, contrary to rocket measurements at these low energies.

Analysing several solar flare events recently Mogro-Compero et al., 1972b and 1973b found a variability in the Fe abundance ratio which is correlated to the CNO/He ratio, in the sense that a He rich event also is rich in iron relative to the C, N, O nuclei. The authors relate the variation to partial

ionization during the acceleration process. If this is true and provided that the charge equilibrium is maintained during the acceleration process, one would expect the strongest energy dependence of the ratio in the energy region, where the ionic charge to mass ratio Q/A of iron and oxygen changes most. But for the October 72 event we see no energy dependence of the Fe/O ratio just in this energy region between few hundred keV/nucleon and several MeV/nucleon.

Our results would suggest just the opposite that at least for this flare during the acceleration process Q/A is the same for both elements and independent of energy. A possibility would be that the particles get accelerated after being fully stripped by energetic electrons in hot flare regions, as proposed by Cartwright et al., 1972 for the 'first step' of their acceleration mechanism. This would imply that the acceleration takes place in a region of the solar atmosphere high enough that the density is sufficiently low that no charge exchange by collision alters the state of ionization and the energy of the particles before escape into the interplanetary space.

Acknowledgements. We wish to thank the staff of the Dept. of Space Physics and Astronomy of the University of Maryland and the Max-Planck-Institut für extraterrestrische Physik (especially to E. Tums, and J. Cain (U. of Md.), and P. Laeverenz, E. Künneth, H. Arbinger, F. Eberl, E. Seidenschwang, and H. Waldleben for their contributions to the management, design and testing of the experiment. We acknowledge the help of J. Dalton and B. Klecker in the data analysis.

5. References.

Bertsch, D.L, C.E. Fichtel, D.V. Reames, Ap. J., 171,169 (1972).
Bertsch, D.L., C.E. Fichtel, C.J. Pelleerin and D.V. Reames, Ap. J., 180, 221, 1973.
Braddy, D., J. Chan, P.B. Price, Phys. Rev. Letters, 30, 669, 1973.
Cartwright, B.G. and A. Mogro-Compero, Ap. J. Letters, 177, L 43 (1972).
Crawford, H.J., P.B. Price, J.D. Sullivan, Ap. J. Letters , 175, L 149, 1972.
Hovestadt, D., O. Vollmer, 12th Internat. Conference on Cosmic Rays, Tech 28, Hobart 1971.
Mogro-Compero, A., J.A. Simpson, Ap. J. Letters, 171, L5 (1972).
Mogro-Compero, A., J.A. Simpson, Ap. J. Letters, 177, L 37, 1972b.
Northcliff, L.C. and R.F. Schilling, Nuclear Data Tables, Vol.7, No. 3-4, p. 233, 1970.
Price, P.B., I. Hutcheon, R. Cowsik, D.J. Barber, Phys. Rev. Letters 26, 916, 1971.
Teegarden, B.J., T.T. von Rosenvinge, F.B. McDonald, Ap. J., 180, 571, 1973.